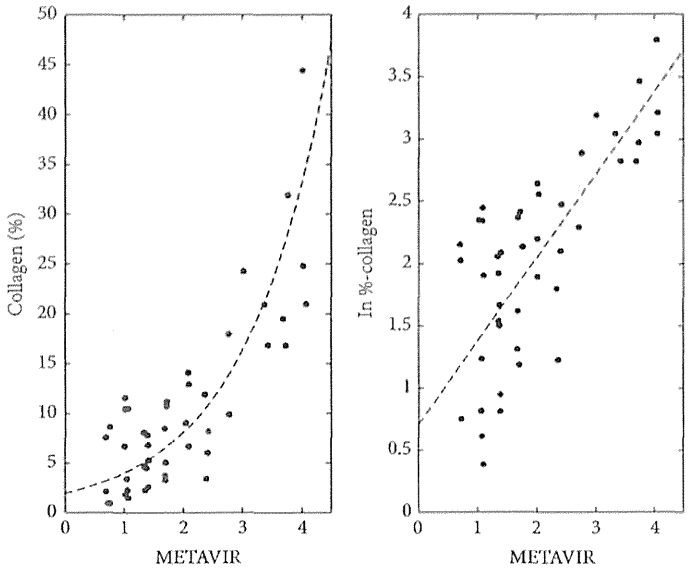

FIGURE 5: Comparison between quantitative versus qualitative histology. Average Metavir of 3 pathology readers versus (a) raw %-collagen (b) and natural logarithm of %-collagen. As shown in (a), the relationship between quantitative and qualitative histology scores is curvilinear. Pearson's correlation coefficient (r) of plot B is 0.81, with $P < 0.001$.

TABLE 2: Fibrosis prediction model parameters (texture versus Metavir).

	Source image	Texture class	Texture feature
1	Original	Pixel intensity histogram	Mean pixel intensity
2	Original	Gaussian mixture model	STD of the lower intensity pixels
3	Original	Gaussian mixture model	AIC of two-Gaussian fit/AIC of single-Gaussian fit
4	Original	Voronoi polygons	STD of the 1st order inertial moment
5	Gradient	Voronoi polygons	Mean of the 2nd order inertial moment
6	Laplacian	Pixel intensity histogram	Mode/interquartile range

Six most predictive texture features, from strongest to weakest. Keys: STD: standard deviation, AIC: Akaike Information Criterion, inertial moments: mathematical description the shape/area of the Voronoi polygons (see supplementary materials).

TABLE 3: Receiver operating characteristics (texture versus Metavir).

Classification	Cutoff	Area under curve	Sensitivity	Specificity	Accuracy
F <1 versus F ≥1	1.805	0.814 [0.654 0.975]	0.659 [0.513 0.804]	0.800 [0.449 1.000]	0.674 [0.524 0.797]
F <2 versus F ≥2	1.916	0.889 [0.783 0.994]	0.895 [0.757 1.000]	0.778 [0.621 0.919]	0.826 [0.686 0.916]
F <3 versus F ≥3	2.060	0.862 [0.701 1.000]	0.778 [0.506 1.000]	0.784 [0.651 0.916]	0.783 [0.615 0.867]
F <4 versus F = 4	2.174	0.976 [0.855 1.000]	1.000 [0.907 1.000]	0.930 [0.854 1.000]	0.935 [0.788 0.974]

Cutoff: the operating point on the ROC curve closest to (0, 1), the point of maximum sensitivity and specificity. [ ]—95% confidence interval. The mismatch between the texture-based cutoff and the histologic classification threshold is expected (see text).

4. Discussion

This study prospectively assessed liver fibrosis in HCV-infected adults noninvasively using quantitative texture analysis of CCE MR images. Liver biopsy was used as the reference standard. Fibrosis severity was scored qualitatively (Metavir) and quantitatively (%-collagen). The study design closely simulated a typical clinical situation, in which a newly diagnosed HCV-positive patient without clinically overt cirrhosis requires assessment of liver fibrosis.

We utilized a CCE MR imaging technique, in which SPIOs and an extracellular Gd-based agent are administered sequentially. Prior studies suggested complimentary effects of SPIO and Gd for visualizing fibrosis. SPIOs accumulate by phagocytosis in Kupffer cells in the hepatic lobules, causing $T2^*$-related negative enhancement. Extracellular Gd-based agents such as Gd-DTPA distribute to the interstitial space of the fibrotic perilobular septa, causing T1-related positive enhancement. The result is a linear meshwork of high-signal perilobular septa against a background of low-signal lobules,

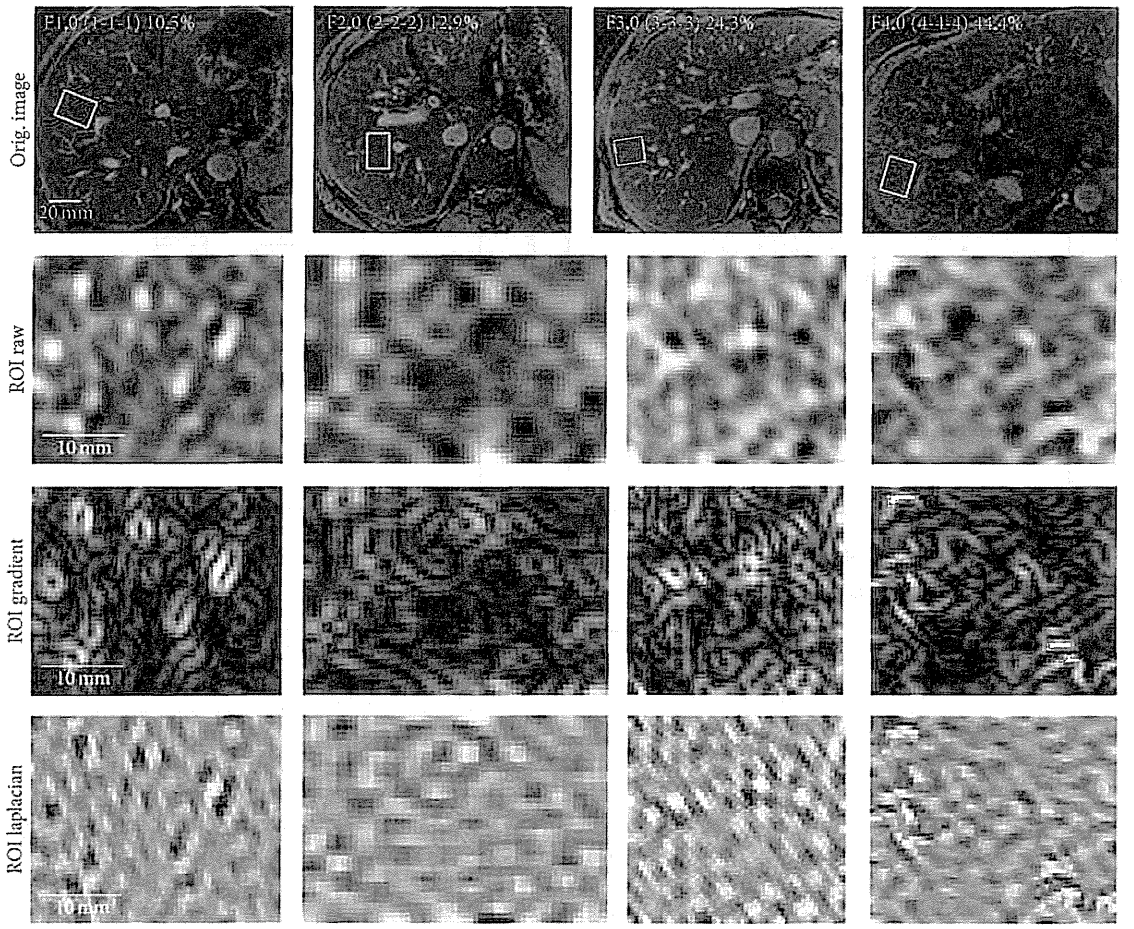

FIGURE 6: Regions-of-interest on CCE MR images in four subjects. Regions-of-interest drawn on CCE MR images in four representative subjects. Average Metavir (and individual reader METAVIR) and %-collagen scores are shown. Subjectively, high-signal reticular texture becomes increasingly conspicuous and disorganized with increasing Metavir and %-collagen scores. CCE: combined contrast enhanced.

TABLE 4: Fibrosis prediction model parameters (texture versus %-collagen).

	Source image	Texture class	Texture feature
1	Original	Gaussian mixture model	STD of the lower intensity pixels
2	Original	Voronoi polygons	Mean of the 2nd order inertial moment
3	Original	Voronoi polygons	STD of the 1st order inertial moment
4	Gradient	Voronoi polygons	Mean of the 2nd order inertial moment
5	Gradient	Gaussian mixture model	STD of the lower intensity pixels
6	Laplacian	Voronoi polygons	Mean of the 3rd order inertial moment

Six most predictive texture features, from strongest to weakest. Keys: STD: standard deviation, AIC: Akaike Information Criterion, inertial moments: mathematical description the shape/area of the Voronoi polygons (see supplementary materials).

TABLE 5: Receiver operating characteristics (texture versus %-collagen).

Classification	Cutoff	Area under curve	Sensitivity	Specificity	Accuracy
<5% versus ≥5%	9.315	0.806 [0.680 0.932]	0.688 [0.527 0.848]	0.857 [0.674 1.000]	0.739 [0.592 0.850]
<10% versus ≥10%	9.807	0.742 [0.589 0.895]	0.722 [0.515 0.929]	0.679 [0.506 0.852]	0.696 [0.547 0.815]
<15% versus ≥15%	10.500	0.894 [0.758 1.000]	0.900 [0.714 1.000]	0.750 [0.609 0.891]	0.783 [0.638 0.884]
<20% versus ≥20%	11.234	0.950 [0.826 1.000]	1.000 [0.907 1.000]	0.825 [0.707 0.943]	0.848 [0.686 0.916]

Cutoff: the operating point on the ROC curve closest to (0, 1), the point of maximum sensitivity and specificity. [ ]—95% confidence interval. The mismatch between the texture-based cutoff and the histologic classification threshold is expected (see text).

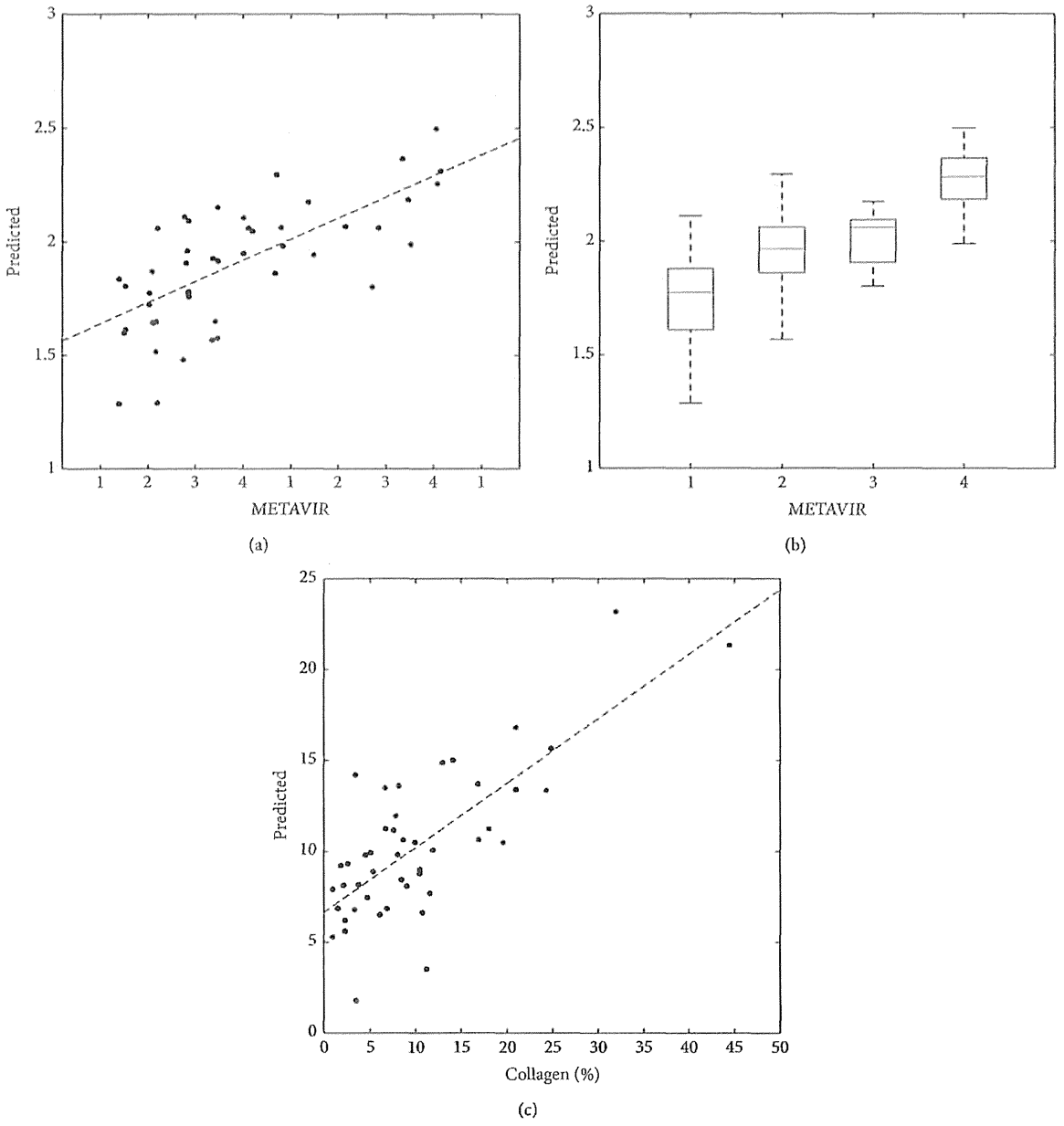

FIGURE 7: Texture versus histologic fibrosis scores. (a) The correlation between the texture and qualitative histology score (average Metavir) is statistically significant with 0.698 ($P < 0.001$) with best-fit line of slope 1.546 and intercept 0.186. (b) Box-plot of texture score versus rounded average Metavir. Spearman's correlation is significant at $\rho = 0.635$ ($P < 0.001$). (c) The correlation between texture and quantitative histology score (percent-fibrosis) is statistically significant with 0.767 ($P < 0.001$), with best-fit line of slope 0.355 and intercept 6.636. The nonunit slope and nonzero intercept are attributable in part to the regularization procedure employed by the GLM-path algorithm (see text).

producing a reticular texture pattern that subjectively becomes more conspicuous with increasing fibrosis severity [26, 27].

We found that CCE MR image texture of the liver can be objectively quantified to predict fibrosis severity. The abnormal texture was detectable at early fibrosis stage, for example, F > 2 Metavir score or >15%-collagen with accuracy of 0.826 and 0.783, respectively. The predicted fibrosis scores correlated with but did not exactly match the corresponding histologically determined scores. The imperfect agreement between predicted and actual fibrosis scores is likely due to three factors: intrinsic inaccuracy of the texture-based technique used in our study, expected mismatch due to the regularization procedure employed by GLM-path (explained earlier), and intrinsic inaccuracy of liver biopsy as a reference standard (explained later).

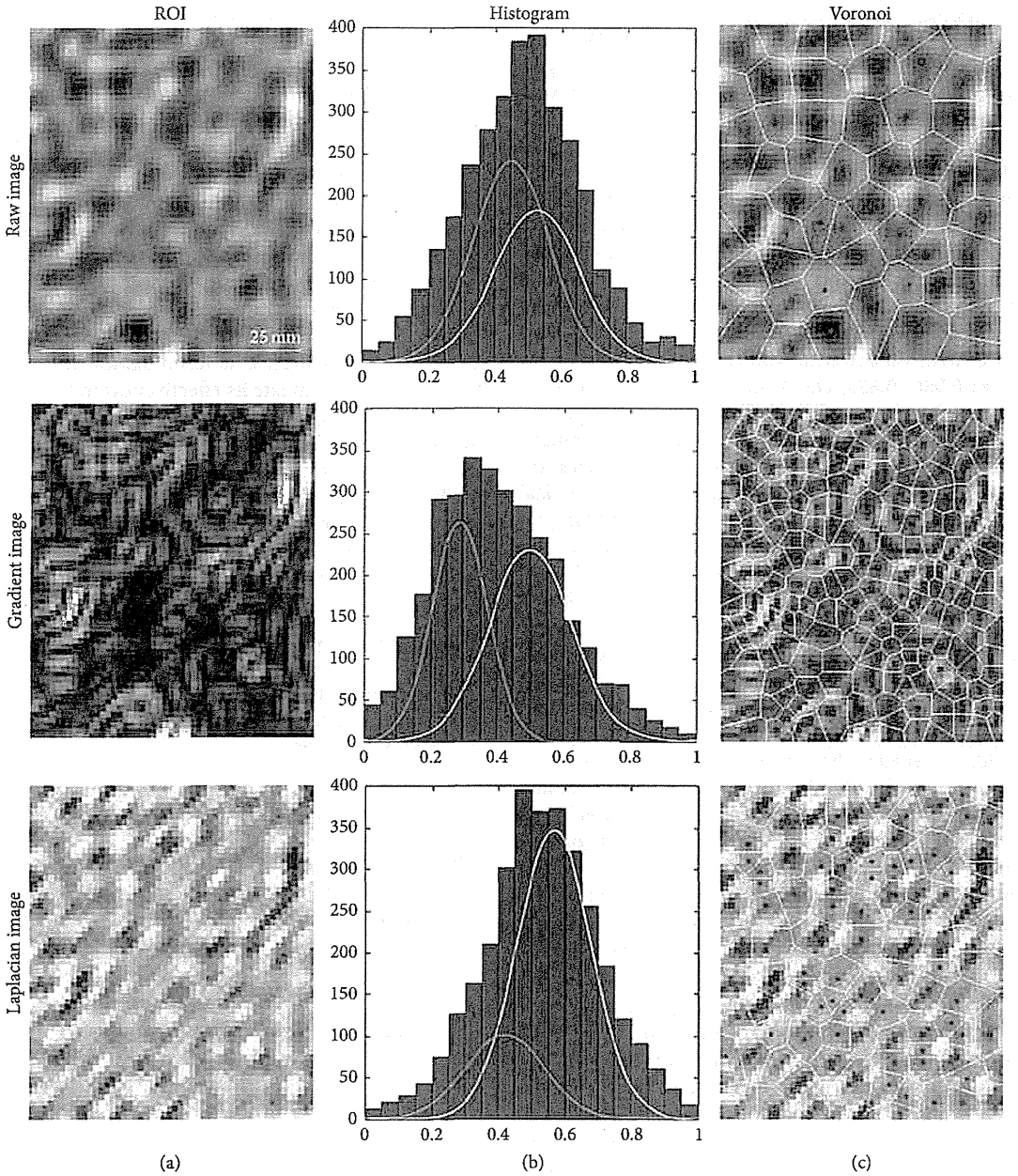

FIGURE 8: Illustrative examples of texture feature classes for fibrosis prediction. A 54 year-old female with cirrhosis. (c) Standardized regions of interest (ROI) images, without transformation (raw), with gradient and Laplacian transformations. (b) Corresponding pixel intensity histogram and its Gaussian mixture model fit with two normal populations. (a) Voronoi polygons constructed on the corresponding ROI images. These texture classes were found to be predictive of liver fibrosis on CCE images (see text). For each texture class (intensity histogram, Gaussian mixture, and Voronoi polygons), relevant statistics were calculated as detailed in supplementary materials and were used for fibrosis prediction.

Gaussian mixture models and Voronoi polygons were found to be predictive texture classes by both qualitative and quantitative histology prediction models. This is consistent with the postulated complimentary effects of SPIO and Gd producing the reticular enhancement pattern in fibrotic livers. A Gaussian mixture model fits two normal distributions, each with its own mean and variance, to the overall pixel intensity histogram. On a CCE image, the liver contains two populations of pixels, one comprised of low-signal SPIO-containing pixels devoid of fibrosis and the other of high-signal Gd-containing pixels in fibrotic septa. With progression of fibrosis, the proportion of high-signal Gd-containing

pixels (i.e., fibrosis) increases and, therefore, the pixel intensity histogram is better fitted by a mixture of two Gaussian distributions than a single Gaussian. The Voronoi polygon algorithm generates a tessellation of polygons that "carves" the liver parenchyma into low-intensity nodules, thereby objectively modeling the reticular texture seen subjectively in progressive fibrosis.

Another MR-based technique, MR elastography (MRE), is increasing in popularity and availability for noninvasive assessment of liver fibrosis. This technique measures the biomechanical stiffness of the liver, which increases as a consequence of fibrosis [38]. In a retrospective study in HCV-infected population [39], the reported AUC, sensitivity, and specificity of MRE in detecting clinically significant fibrosis ($F \geq 2$) was 0.986, 0.885, and 1.00, respectively, similar to slightly higher than those of the CCE texture method. However, texture-based methods may have a theoretical advantage of more direct visualization of fibrosis while MRE measures the tissue biomechanical sequela of fibrosis. Another practical advantage of texture-based methods is that they can be implemented on any clinical scanner using standard sequences, while MRE requires dedicated hardware (mechanical wave transducer) and sequences. Disadvantages of texture-based methods are the need for intravenous access and injection of contrast agents, including two agents for the CCE technique described here. Also, visualization of subtle reticulations associated with early fibrosis is sensitive to patient motion; consequently we obtained four CCE image sets in separate breath-holds, to ensure that at least one set was motion-free. As motion correction/minimization techniques become more robust and clinically available, it may be possible to acquire images during free breathing with higher signal-to-noise ratio and spatial resolution.

A limitation of this study is the use of single liver biopsy as the reference standard. A typical core biopsy (~30 mm^3) samples only 1/50,000 of the liver and is significantly smaller than the imaging ROI (>400 mm^3) used in the texture analysis. Also, biopsied sites are difficult to colocalize with imaging ROIs, which is relevant because the severity of fibrosis can be heterogeneous across the liver. An error frequency of up to 33% has been reported for differences in ≥ one fibrosis stage and cirrhosis may be missed in 10–30% of blind biopsies [40]. Thus even a "perfect" fibrosis prediction method may have only moderate observed accuracy in binary classification if single-biopsy histology is used as the reference. Obtaining multiple biopsies may reduce errors in the reference standard, but increases the complication risk and was not feasible in this study. Considering these limitations, moderate accuracy of CCE MR imaging is appropriate and expected. Determination of the true accuracy of fibrosis imaging may require histologic evaluation of larger specimens than those obtained by percutaneous biopsy. Another consideration for the accuracy of biopsy as the reference standard is observer bias [10]. To minimize the observer bias and increase the accuracy of fibrosis staging, this study used the average Metavir score of three hepatopathologists' independent interpretations as the reference standard. While averaging of an ordinal fibrosis score is less than ideal, it is arguably the most valid fibrosis severity metric available from a single biopsy specimen. Such a practice is not uncommon in hepatology literature [41–44]. As average Metavir score is expected to preserve the rank-order relationship of the fibrosis severity, it should be sufficient to mathematically construct a valid fibrosis prediction model.

While this study suggested a promising indication for SPIO agents in liver fibrosis imaging, ferumoxides were withdrawn from the US market in 2009. Recently, another intravenously injectable SPIO-based drug, ferumoxytol (Feraheme, AMAG Pharmaceuticals, Lexington, MA) has been FDA-approved for iron-deficiency therapy and early data on its application as contrast agent for MR imaging are promising [45]. While this new drug likely has similar negative-contrast effects in the liver as ferumoxides, further studies will be necessary to evaluate its effectiveness in CCE imaging.

In summary, this proof-of-concept prospective study showed that CCE MR imaging and quantitative texture analysis may permit noninvasive assessment of liver fibrosis in HCV-infected adults. MR image texture is a potential noninvasive biomarker of liver fibrosis and, with further technical refinement and validation, may provide a new tool in clinical management and research in HCV-infected patients.

Conflict of Interests

The contents of this work are solely the responsibility of the authors and do not necessarily represent the official views of the funding agencies.

Acknowledgments

This work was funded in part by grants from the Radiological Society of North America R&E Foundation Research Resident Award no. RR0726, the National Institutes of Health NCMHD EXPORT P60 MD00220, and Bayer Healthcare Grant no. 070525.

References

[1] K. D. Kochanek, S. L. Murphy, R. N. Anderson, and C. Scott, "Deaths: final data for 2002," *National Vital Statistics Reports*, vol. 53, no. 5, pp. 1–115, 2004.

[2] Y.-S. Lim and W. R. Kim, "The global impact of hepatic fibrosis and end-stage liver disease," *Clinics in Liver Disease*, vol. 12, no. 4, pp. 733–746, 2008.

[3] S. Vong and B. P. Bell, "Chronic liver disease mortality in the United States, 1990–1998," *Hepatology*, vol. 39, no. 2, pp. 476–483, 2004.

[4] G. L. Armstrong, A. Wasley, E. P. Simard, G. M. McQuillan, W. L. Kuhnert, and M. J. Alter, "The prevalence of hepatitis C virus infection in the United States, 1999 through 2002," *Annals of Internal Medicine*, vol. 144, no. 10, pp. 705–714, 2006.

[5] I. M. Arias, *The Liver: Biology and Pathobiology*, John Wiley & Sons, Chichester, UK, 5th edition, 2009.

[6] L. Peters and J. K. Rockstroh, "Biomarkers of fibrosis and impaired liver function in chronic hepatitis C: how well do they predict clinical outcomes?" *Current Opinion in HIV and AIDS*, vol. 5, no. 6, pp. 517–523, 2010.

[7] G. Germani, P. Hytiroglou, A. Fotiadu, A. K. Burroughs, and A. P. Dhillon, "Assessment of fibrosis and cirrhosis in liver biopsies: an update," *Seminars in Liver Disease*, vol. 31, no. 1, pp. 82–90, 2011.

[8] P. Marcellin, "Hepatitis B and hepatitis C in 2009," *Liver International*, vol. 29, supplement 1, pp. 1–8, 2009.

[9] P. Bedossa and T. Poynard, "An algorithm for the grading of activity in chronic hepatitis C," *Hepatology*, vol. 24, no. 2, pp. 289–293, 1996.

[10] "Intraobserver and interobserver variations in liver biopsy interpretation in patients with chronic hepatitis C. The French METAVIR Cooperative Study Group," *Hepatology*, vol. 20, no. 1, part 1, pp. 15–20, 1994.

[11] J. Perrault, D. B. McGill, B. J. Ott, and W. F. Taylor, "Liver biopsy: complications in 1000 inpatients and outpatients," *Gastroenterology*, vol. 74, no. 1, pp. 103–106, 1978.

[12] P. Thampanitchawong and T. Piratvisuth, "Liver biopsy: complications and risk factors," *World Journal of Gastroenterology*, vol. 5, no. 4, pp. 301–304, 1999.

[13] P. Halfon, F. Imbert-Bismut, D. Messous et al., "A prospective assessment of the inter-laboratory variability of biochemical markers of fibrosis (FibroTest) and activity (ActiTest) in patients with chronic liver disease," *Comparative Hepatology*, vol. 1, article 3, 2002.

[14] E. Rossi, L. Adams, A. Prins et al., "Validation of the FibroTest biochemical markers score in assessing liver fibrosis in hepatitis C patients," *Clinical Chemistry*, vol. 49, no. 3, pp. 450–454, 2003.

[15] H. Saito, S. Tada, N. Nakamoto et al., "Efficacy of non-invasive elastometry on staging of hepatic fibrosis," *Hepatology Research*, vol. 29, no. 2, pp. 97–103, 2004.

[16] A. Ziolkowski, M. Wylezol, M. Kukla et al., "The comparison of scoring scales for liver biopsy assessment in morbidly obese patients undergoing bariatric surgery," *Obesity Surgery*, vol. 15, no. 9, pp. 1309–1314, 2005.

[17] L. Huwart, F. Peeters, R. Sinkus et al., "Liver fibrosis: non-invasive assessment with MR elastography," *NMR in Biomedicine*, vol. 19, no. 2, pp. 173–179, 2006.

[18] O. Rouvière, M. Yin, M. A. Dresner et al., "MR elastography of the liver: preliminary results," *Radiology*, vol. 240, no. 2, pp. 440–448, 2006.

[19] M. Yin, J. A. Talwalkar, K. J. Glaser et al., "Assessment of hepatic fibrosis with magnetic resonance elastography," *Clinical Gastroenterology and Hepatology*, vol. 5, no. 10, pp. 1207.e2–1213.e2, 2007.

[20] C. Aubé, P. X. Racineux, J. Lebigot et al., "Diagnosis and quantification of hepatic fibrosis with diffusion weighted MR imaging: preliminary results," *Journal de Radiologie*, vol. 85, no. 3, pp. 301–306, 2004.

[21] M. Koinuma, I. Ohashi, K. Hanafusa, and H. Shibuya, "Apparent diffusion coefficient measurements with diffusion-weighted magnetic resonance imaging for evaluation of hepatic fibrosis," *Journal of Magnetic Resonance Imaging*, vol. 22, no. 1, pp. 80–85, 2005.

[22] J. A. Talwalkar, M. Yin, J. L. Fidler, S. O. Sanderson, P. S. Kamath, and R. L. Ehman, "Magnetic resonance imaging of hepatic fibrosis: emerging clinical applications," *Hepatology*, vol. 47, no. 1, pp. 332–342, 2008.

[23] G. Elizondo, R. Weissleder, D. D. Stark et al., "Hepatic cirrhosis and hepatitis: MR imaging enhanced with superparamagnetic iron oxide," *Radiology*, vol. 174, no. 3, pp. 797–801, 1990.

[24] T. Fujita, K. Ito, K. Honjo, H. Okazaki, T. Matsumoto, and N. Matsunaga, "Hepatic parenchymal enhancement in the cirrhotic liver: evaluation by triple-phase dynamic MRI," *Abdominal Imaging*, vol. 27, no. 1, pp. 29–33, 2002.

[25] K. M. Vitellas, M. T. Tzalonikou, W. F. Bennett, K. K. Vaswani, and J. G. Bova, "Cirrhosis: spectrum of findings on unenhanced and dynamic gadolinium-enhanced MR imaging," *Abdominal Imaging*, vol. 26, no. 6, pp. 601–615, 2001.

[26] D. A. Aguirre, C. A. Behling, E. Alpert, T. I. Hassanein, and C. B. Sirlin, "Liver fibrosis: noninvasive diagnosis with double contrast material-enhanced MR imaging," *Radiology*, vol. 239, no. 2, pp. 425–437, 2006.

[27] F. Hughes-Cassidy, A. D. Chavez, A. Schlang et al., "Superparamagnetic iron oxides and low molecular weight gadolinium chelates are synergistic for direct visualization of advanced liver fibrosis," *Journal of Magnetic Resonance Imaging*, vol. 26, no. 3, pp. 728–737, 2007.

[28] H. Kato, M. Kanematsu, X. Zhang et al., "Computer-aided diagnosis of hepatic fibrosis: preliminary evaluation of MRI texture analysis using the finite difference method and an artificial neural network," *American Journal of Roentgenology*, vol. 189, no. 1, pp. 117–122, 2007.

[29] G. Bahl, D. A. Aguirre, G. Motta, A. Fotinos, G. Rescinito, and C. Sirlin, "Quantitative texture analysis of liver fibrosis on double-contrast enhanced gradient recalled echo images," in *Proceedings of the RSNA Annual Meeting*, Chicago, Ill, USA, 2005.

[30] G. Bahl, I. Cruite, T. Wolfson et al., "Noninvasive classification of hepatic fibrosis based on texture parameters from double contrast-enhanced magnetic resonance images," *Journal of Magnetic Resonance Imaging*, vol. 36, no. 5, pp. 1154–1161, 2012.

[31] P. F. Hahn and S. Saini, "Liver-specific MR imaging contrast agents," *Radiologic Clinics of North America*, vol. 36, no. 2, pp. 287–297, 1998.

[32] Y. Gandon, J.-F. Heautot, F. Brunet, D. Guyader, Y. Deugnier, and M. Carsin, "Superparamagnetic iron oxide: clinical time-response study," *European Journal of Radiology*, vol. 12, no. 3, pp. 195–200, 1991.

[33] S. Aime and P. Caravan, "Biodistribution of gadolinium-based contrast agents, including gadolinium deposition," *Journal of Magnetic Resonance Imaging*, vol. 30, no. 6, pp. 1259–1267, 2009.

[34] M. Y. Park and T. Hastie, "L_1-regularization path algorithm for generalized linear models," *Journal of the Royal Statistical Society B*, vol. 69, no. 4, pp. 659–677, 2007.

[35] H. Akaike, "A new look at the statistical model identification," *IEEE Transactions on Automatic Control*, vol. 19, no. 6, pp. 716–723, 1974.

[36] V. Calvaruso, A. K. Burroughs, R. Standish et al., "Computer-assisted image analysis of liver collagen: relationship to Ishak scoring and hepatic venous pressure gradient," *Hepatology*, vol. 49, no. 4, pp. 1236–1244, 2009.

[37] M. J. O'Brien, N. M. Keating, S. Elderiny et al., "An assessment of digital image analysis to measure fibrosis in liver biopsy specimens of patients with chronic hepatitis C," *The American Journal of Clinical Pathology*, vol. 114, no. 5, pp. 712–718, 2000.

[38] S. K. Venkatesh and R. L. Ehman, "Magnetic resonance elastography of liver," *Magnetic Resonance Imaging Clinics of North America*, vol. 22, no. 3, pp. 433–446, 2014.

[39] S. Ichikawa, U. Motosugi, T. Ichikawa et al., "Magnetic resonance elastography for staging liver fibrosis in chronic hepatitis C," *Magnetic Resonance in Medical Sciences*, vol. 11, no. 4, pp. 291–297, 2012.

[40] D. S. Manning and N. H. Afdhal, "Diagnosis and quantitation of fibrosis," *Gastroenterology*, vol. 134, no. 6, pp. 1670–1681, 2008.

[41] M. L. Shiffman, R. T. Stravitz, M. J. Contos et al., "Histologic recurrence of chronic hepatitis C virus in patients after living donor and deceased donor liver transplantation," *Liver Transplantation*, vol. 10, no. 10, pp. 1248–1255, 2004.

[42] J. C. Hoefs, M. L. Shiffman, Z. D. Goodman, D. E. Kleiner, J. L. Dienstag, and A. M. Stoddard, "Rate of progression of hepatic fibrosis in patients with chronic hepatitis C: results from the HALT-C trial," *Gastroenterology*, vol. 141, no. 3, pp. 900.e2–908.e2, 2011.

[43] A. Monto, S. Kakar, L. M. Dove, A. Bostrom, E. L. Miller, and T. L. Wright, "Contributions to hepatic fibrosis in HIV-HCV coinfected and HCV monoinfected patients," *The American Journal of Gastroenterology*, vol. 101, no. 7, pp. 1509–1515, 2006.

[44] R. Malekzadeh, M. Mohamadnejad, and N. Rakhshani, "Reversibility of cirrhosis in chronic hepatitis B," *Clinical Gastroenterology and Hepatology*, vol. 2, no. 4, pp. 344–347, 2004.

[45] M. R. Bashir, L. Bhatti, D. Marin, and R. C. Nelson, "Emerging applications for ferumoxytol as a contrast agent in MRI," *Journal of Magnetic Resonance Imaging*, 2014.

FEBS Open Bio 4 (2014) 777–787

ELSEVIER

FEBS openbio

journal homepage: www.elsevier.com/locate/febsopenbio

Necrostatin-1 protects against reactive oxygen species (ROS)-induced hepatotoxicity in acetaminophen-induced acute liver failure

Kenji Takemoto [a,b], Etsuro Hatano [b,*], Keiko Iwaisako [c], Masatoshi Takeiri [a], Naruto Noma [a], Saori Ohmae [a], Kan Toriguchi [b], Kazutaka Tanabe [b], Hirokazu Tanaka [b], Satoru Seo [b], Kojiro Taura [b], Keigo Machida [d], Norihiko Takeda [e], Shigehira Saji [c], Shinji Uemoto [b], Masataka Asagiri [a,*]

[a] Innovation Center for Immunoregulation and Therapeutics, Graduate School of Medicine, Kyoto University, Yoshida Konoe, Sakyo-ku, Kyoto 606-8501, Japan
[b] Division of Hepato-Biliary-Pancreatic Surgery and Transplantation, Department of Surgery, Graduate School of Medicine, Kyoto University, 54 Kawaharacho, Syogoin, Sakyo-ku, Kyoto 606-8507, Japan
[c] Department of Target Therapy Oncology, Graduate School of Medicine, Kyoto University, 54 Kawaharacho, Syogoin, Sakyo-ku, Kyoto 606-8507, Japan
[d] Molecular Microbiology and Immunology, Keck School of Medicine, University of Southern California, 1975 Zonal Ave, Los Angeles, CA 90033, USA
[e] Department of Cardiovascular Medicine, Graduate School of Medicine, The University of Tokyo, 7-3-1 Hongo, Bunkyo-ku, Tokyo 113-8655, Japan

ARTICLE INFO

Article history:
Received 30 April 2014
Revised 29 August 2014
Accepted 30 August 2014

Keywords:
Hepatocytes
Acetaminophen
Acute liver failure
RIPK-dependent necrosis
Necroptosis
Reactive oxygen species

ABSTRACT

Excessive acetaminophen (APAP) use is one of the most common causes of acute liver failure. Various types of cell death in the damaged liver are linked to APAP-induced hepatotoxicity, and, of these, necrotic cell death of hepatocytes has been shown to be involved in disease pathogenesis. Until recently, necrosis was commonly considered to be a random and unregulated form of cell death; however, recent studies have identified a previously unknown form of programmed necrosis called receptor-interacting protein kinase (RIPK)-dependent necrosis (or necroptosis), which is controlled by the kinases RIPK1 and RIPK3. Although RIPK-dependent necrosis has been implicated in a variety of disease states, including atherosclerosis, myocardial organ damage, stroke, ischemia–reperfusion injury, pancreatitis, and inflammatory bowel disease. However its involvement in APAP-induced hepatocyte necrosis remains elusive. Here, we showed that RIPK1 phosphorylation, which is a hallmark of RIPK-dependent necrosis, was induced by APAP, and the expression pattern of RIPK1 and RIPK3 in the liver overlapped with that of CYP2E1, whose activity around the central vein area has been demonstrated to be critical for the development of APAP-induced hepatic injury. Moreover, a RIPK1 inhibitor ameliorated APAP-induced hepatotoxicity in an animal model, which was underscored by significant suppression of the release of hepatic enzymes and cytokine expression levels. RIPK1 inhibition decreased reactive oxygen species levels produced in APAP-injured hepatocytes, whereas CYP2E1 expression and the depletion rate of total glutathione were unaffected. Of note, RIPK1 inhibition also conferred resistance to oxidative stress in hepatocytes. These data collectively demonstrated a RIPK-dependent necrotic mechanism operates in the APAP-injured liver and inhibition of this pathway may be beneficial for APAP-induced fulminant hepatic failure.

1. Introduction

Acetaminophen, or N-acetyl-para-amino-phenol (APAP), is the most widely used analgesic and antipyretic [1]. The use of APAP is safe at therapeutic doses, but high doses can lead to acute liver failure (ALF). In 1998, 28% of all ALF cases in the United States were attributed to APAP overdose, which increased to 51% in 2003 [2]. Furthermore, the percentage was much higher in the United Kingdom, where 57% of ALF cases were attributed to APAP use from 1999 to 2008 [3]. The toxicity of APAP is ascribed to N-acetyl-p-benzoquinone imine (NAPQI), a highly reactive metabolite of APAP, which reacts with glutathione (GSH) and leads to a profound depletion of hepatocellular GSH [4], resulting in mitochondrial

Abbreviations: ABTS, 2,2′-azino-bis (3-ethylbenzothiazoline)-6-sulfonic acid; ALF, acute liver failure; ALT, alanine aminotransferase; APAP, acetaminophen; AST, aspartate aminotransferase; bFGF, basic fibroblast growth factor; CM-H_2DCFDA, 5-(and-6)-chloromethyl-2′,7′-dichlorodihydrofluorescein diacetate, acetyl ester; CXCL1, chemokine (C-X-C motif) ligand 1; CYP2E1, cytochrome P450 2E1; DMSO, dimethyl sulfoxide; Drp1, dynamin-related protein 1; FBS, fetal bovine serum; GSH, glutathione; LDH, lactate dehydrogenase; NAPQI, N-acetyl-p-benzoquinone; Nec-1, necrostatin-1; NO, nitric oxide; PGAM5, phosphoglycerate mutase family member 5; PI, propidium iodide; RIPK, receptor-interacting protein kinase; ROS, reactive oxygen species; SNAP, S-nitroso-N-acetyl-DL-penicillamine; WST-8, 2-(2-methoxy-4-nitrophenyl)-3-(4-nitrophenyl)-5-(2,4-disulfophenyl)-2H-tetrazolium; λPP, lambda protein phosphatase

* Corresponding authors. Tel.: +81 75 751 4323; fax: +81 75 751 4263 (E. Hatano). Tel.: +81 75 753 9502; fax: +81 75 753 9500 (M. Asagiri).
E-mail addresses: etsu@kuhp.kyoto-u.ac.jp (E. Hatano), masa-asagiri@umin.org (M. Asagiri).

http://dx.doi.org/10.1016/j.fob.2014.08.007
2211-5463/

permeability transition and necrotic cell death [5]. Of note, although necrosis is the major contributing mechanism of APAP-induced hepatic injury [6], various types of cell death resulting from several complicated mechanisms are assumed to play a role in this process [7].

Necrosis has been considered as an accidental and non-regulated cell death process; however, recent studies have shed light on a new concept of regulated necrosis called receptor-interacting protein kinase (RIPK)-dependent necrosis (or necroptosis). The most prominent characteristics of this type of cell death are as follows: (i) RIPK1 kinase activation, which can be assessed by monitoring RIPK1 phosphorylation, and (ii) cell-death, which can be suppressed by several RIPK1 inhibitors, including necrostatin-1 (Nec-1) [8]. Necroptosis results from RIPK1 and RIPK3 kinase activity in the form of a necrosome, which is regulated by ubiquitination and phosphorylation of RIPK1 and RIPK3 [9]. RIPK1–RIPK3 necrosome formation, which is induced by several factors, including tumor necrosis factor alpha (TNF), leads to the overproduction of reactive oxygen species (ROS) and the induction of mitochondrial dysfunction mediated by mitochondrial complex I [10]. Furthermore, the mitochondrial phosphatase PGAM5 and the mitochondrial fission factor Drp1, which cause mitochondrial fragmentation and may up-regulate ROS generation, are intimately involved in RIPK-dependent necrosis [11]. Nec-1 allosterically blocks RIPK1 kinase activity and inhibits RIPK-dependent necrosis, though the activation of RIPK1-mediated NF-κB, mitogen-activated protein kinase p38 and JNK1 remain [12,13]. Nec-1 blocks the formation of the RIPK1–RIPK3 complex, indicating that kinase activity of RIPK1 is required for necrosome formation [13]. The cytoprotective effects of Nec-1 has been shown in several experimental settings, in ischemic brain injury [14], myocardial ischemia–reperfusion [15], as well as radiation-induced cell death in anaplastic thyroid and adrenocortical cancers [16].

Here, we studied the molecular mechanisms involved in APAP-induced ALF and found that RIPK-dependent necrosis is involved in APAP-induced hepatocyte death, suggesting that hepatotoxicity is, at least partly, due to druggable cellular events. Indeed, we also provide evidence that Nec-1 successfully protects against APAP-induced acute hepatotoxicity through the acquisition of resistance to oxidative stress as well as by suppressing ROS production in hepatocytes.

2. Materials and methods

2.1. Animals

Male C57BL/6 mice, 8–10 weeks old, were purchased from CLEA Japan (Tokyo, Japan). To confirm the time-dependent development of hepatotoxicity and the involvement of RIPK1 activation in APAP-induced hepatotoxicity, overnight-fasted mice received a single intraperitoneal injection of 800 mg/kg APAP (Sigma–Aldrich, St. Louis, MO, USA) and were sacrificed 0, 1, 3, and 6 h after administration. To investigate the outcome of RIPK1 inhibition, fasted mice received an intravenous injection of 12.5 mg/kg Nec-1 (Calbiochem, San Diego, CA, USA), which was dissolved in dimethyl sulfoxide (DMSO) diluted in a warm saline solution. Control mice were intravenously injected with the same volume of DMSO in a warm saline solution, because DMSO reduces APAP-induced liver damage [17]. All mice received an intraperitoneal injection of 800 mg/kg acetaminophen dissolved in warm saline 15 min after pretreatment with Nec-1 or DMSO, and were sacrificed 6 h after administration. Blood was collected from the vena cava under general anesthesia, and serum was separated to measure aspartate aminotransferase (AST), alanine aminotransferase (ALT), and lactate dehydrogenase (LDH). Portions of the liver tissue specimens were frozen immediately in liquid nitrogen for further use, and the remaining portions were fixed in 10% neutral buffered formalin for microscopic analysis. The Animal Research Committee of Kyoto University approved the animal protocol, and all experiments were conducted in accordance with the Guidelines for the Care and Use of Laboratory Animals promulgated by the National Institutes of Health.

2.2. Immunohistochemical analysis

Formalin-fixed, paraffin-embedded sections were cut into a thickness of 4 μm and mounted on Matsunami adhesive silane-coated glass slides (Matsunami Glass, Osaka, Japan). After deparaffinization and rehydration, the slides were autoclaved in 10 mM citrate buffer for 20 min to retrieve the antigens. Then, endogenous peroxidase was quenched with 0.3% hydrogen peroxide (H_2O_2) in methanol at room temperature for 10 min. After blocking, the sections were incubated at 4 °C overnight with the following primary diluted antibodies: anti-CYP2E1 (dilution, 1:500; Abcam, Cambridge, UK), anti-RIPK1 (dilution, 1:200; Santa Cruz Biotechnology, Dallas, TX, USA), and anti-RIPK3 (dilution, 1:300; Imgenex, San Diego, CA, USA). Subsequently, the sections were incubated with peroxidase-labeled polymer conjugated secondary antibody (Dako Japan, Tokyo, Japan) for 30 min at room temperature. Immunoreactivity was detected with a diaminobenzidine substrate kit (Dako Japan), and the sections were counterstained with hematoxylin. ImageJ imaging analysis software (National Institutes of Health, Bethesda, MD, USA) was used to quantitate the percentage of necrotic area. Field images at ×100 magnification were selected at random from different individuals. The percentage of necrosis was determined by measuring the total dimension of the field and comparing it with the dimension of the necrotic area.

2.3. Measurement of inflammatory and regenerative cytokines

The frozen mouse liver tissues were homogenized using the FastPrep-24 tissue homogenizer (MP Biomedicals Japan, Tokyo, Japan) with 2.0 mm zirconia beads for 1 min while cooling. Bio-Plex multiplex system (Bio-Rad Laboratories, Hercules, CA, USA) was used in conjunction with the Bio-Plex 200 (Bio-Rad Laboratories) to measure inflammatory mediators, according to the manufacturer's directions. Data were analyzed using Bio-Plex Manager 6.1 software (Bio-Rad Laboratories).

2.4. Isolation and culture of primary mouse hepatocytes

Primary hepatocytes were isolated from C57BL/6 mice as described previously [18] and cultured on a collagen-coated plastic dish in Williams' medium E (Life Technologies, Carlsbad, CA, USA) containing 10% fetal bovine serum (FBS), 2 mM L-glutamine, 100 U/mL penicillin, and 100 μg/mL streptomycin at 37 °C in a humidified atmosphere of 5% CO_2. The medium was replaced with serum-free Williams' medium E, including the vehicle (0.05% DMSO) or each of the tested Nec-1 concentrations 3 h after plating. An hour later, the cells were treated with 10 mM APAP (Sigma–Aldrich) and incubated for an additional 18 h. The APAP incubation period was relatively short after isolation, because cultured hepatocytes have less CYP2E1 and are less sensitive to APAP with time [19].

2.5. Cell death assay

Cell death was assayed by measuring LDH in the supernatant using the Cytotoxicity Detection Kit Plus (Roche Diagnostics GmbH, Mannheim, Germany). Then, the cells were incubated for 60–120 min with 2-(2-methoxy-4-nitrophenyl)-3-(4-nitrophenyl)-5-(2,4-disulfophenyl)-2H-tetrazolium (WST-8; Dojindo Laboratories, Kumamoto, Japan) reagent supplemented in culture

media prior to absorbance readings at 450 nm with an iMark Microplate Absorbance Reader (Bio-Rad Laboratories). Thereafter, the cells were stained with Hoechst 33342 (Dojindo Laboratories) and propidium iodide (PI; Dojindo Laboratories). PI-positive cells were considered as dead cells.

2.6. Total GSH measurements

GSH levels in cultured hepatocytes treated with or without APAP were determined using the Total Glutathione Quantification Kit (Dojindo Laboratories), according to the manufacturer's instructions. Each GSH value was expressed as a ratio of the control value.

2.7. ROS measurements

ROS content was quantified using the fluorescent dye 5-(and-6)-chloromethyl-2′,7′-dichlorodihydrofluorescein diacetate, acetyl ester (CM-H_2DCFDA) (Life Technologies) as described previously [20]. Hepatocytes were isolated from C57BL/6 mice and cultured in 96-well black plates with transparent bottoms in Williams' medium E containing 10% FBS, 2 mM L-glutamine, 100 U/mL penicillin, and 100 μg/mL streptomycin at 37 °C for 3 h. The cells were then incubated in serum-free media, including 0.05% DMSO and several Nec-1 concentrations for 1 h. Then, 10 mM APAP diluted in serum-free media was added, and the incubation was continued for an additional 6 h. The hepatocytes were subsequently loaded with CM-H_2DCFDA (10 μM) diluted in phenol red and serum-free media for 30 min at 37 °C. The cells were then rinsed twice with Williams' medium E without phenol red. CM-H_2DCFDA fluorescence was detected at excitation and emission wavelengths of 490 nm and 520 nm, respectively. ROS formation was measured over a time period of 60 min using a FlexStation 3 microplate reader (Molecular Devices, Sunnyvale, CA, USA). Hepatic ROS generation was detected microscopically using the MitoSOX Red Mitochondrial Superoxide Indicator (Life Technologies), which selectively targets superoxide production in mitochondria, according to the manufacturer's instructions.

2.8. Protein blotting

Frozen liver tissue or cultured hepatocytes were homogenized in RIPA buffer (Cell Signaling Technology, Danvers, MA, USA) containing benzylsulfonyl fluoride (Tokyo Chemical Industry, Tokyo, Japan), Halt protease inhibitor cocktail (Pierce Biotechnology, Rockford, IL, USA), and PhosSTOP phosphatase inhibitor cocktail (Roche Diagnostics GmbH) or in a buffer containing 20 mM Tris–HCl, 150 mM NaCl, 1% NP-40, 1% sodium deoxycholate, and Halt protease inhibitor cocktail. Aliquots of hepatocyte extracts were fractionated by electrophoresis on a 7.5% or 10% sodium dodecyl sulfate (SDS) polyacrylamide gel (Bio-Rad Laboratories). In some cases, phosphate-affinity gel electrophoresis was performed using gels containing 8.5% acrylamide, 50 μM $MnCl_2$, and 25 μM acrylamide-pendant Phos-tag ligand (NARD Institute, Ltd., Amagasaki, Japan) [21], and an equal aliquot was incubated for 30 min at 30 °C with or without 400 U λPP (New England Biolabs Inc., Ipswich, MA, USA) prior to electrophoresis. The proteins were transferred onto polyvinylidene fluoride membranes (Bio-Rad Laboratories), blocked with Blocking One blocking solution (Nacalai Tesque, Ltd., Kyoto, Japan), and incubated at 4 °C overnight with anti-CYP2E1 (dilution, 1:1000), anti-RIP1 (dilution, 1:1000; Cell Signaling Technology), and anti-β-actin (dilution, 1:1000; Sigma–Aldrich). The membranes were washed and incubated with horseradish peroxidase-conjugated secondary antibodies. Chemiluminescence was detected using Clarity Western ECL substrate (Bio-Rad Laboratories), the membranes were subjected to direct densitometric analysis, and images were captured using a charge-coupled device camera system (LAS-4000 mini; Fujifilm, Tokyo, Japan). Band intensity was quantified using ImageJ software and normalized with respect to β-actin levels as an internal control.

2.9. Cell death induction by an exogenous ROS inducer

To evaluate the effects of ROS on RIPK1-inhibited hepatocytes, the medium was replaced with serum-free Williams' medium E, including the vehicle (0.05% DMSO), or each of the tested Nec-1 concentrations. After 1 h, H_2O_2 (30% v/v; Wako Pure Chemical Industries, Osaka, Japan) or the nitric oxide (NO) donor S-nitroso-N-acetyl-DL-penicillamine (SNAP; Sigma–Aldrich), which was diluted to a final concentration of 250 μM and 2 mM in serum-free Williams' medium E, was added, and the cells were incubated for 6 h. Thereafter, cell death assays were performed.

2.10. 2,2′-Azino-bis (3-ethylbenzothiazoline)-6-sulfonic acid (ABTS) free radical decolorization assay

This spectrophotometric decolorization assay, which is widely used for the assessment of antioxidant activity, measures the loss of color when an antioxidant is added to the blue–green chromophore ABTS radical cation (ABTS•+). The radical scavenging capacity of a sample was previously determined [22] with some modifications. In brief, ABTS (Wako Pure Chemical Industries) was dissolved in UltraPure Distilled Water (Life Technologies) to a concentration of 7 mM. The ABTS radical cation (ABTS•+) was produced by reacting ABTS stock solution at a final concentration of 2.45 mM potassium persulfate and allowing the mixture to stand in the dark at room temperature for 12–16 h before use. Because ABTS and potassium persulfate react stoichiometrically at a ratio of 1:0.5, this will result in incomplete oxidation of the ABTS. Oxidation of the ABTS commenced immediately, but the absorbance was not maximal and stable until more than 6 h had elapsed. The radical was stable in this form for more than two days when stored in the dark at room temperature. The ABTS•+ solution was diluted with UltraPure Distilled Water or ethanol to an absorbance of 0.70–0.80 at 734 nm. After the addition of 100 μL diluted ABTS•+ solution to 20 μL of necrostatin-1, Inactive control (Calbiochem), which is an inactive analogue of Nec-1, or L(+)-Ascorbic Acid (Wako Pure Chemical Industries), absorbance (734 nm) was measured at exactly 4 min after initial mixing using a FlexStation 3 microplate reader (Molecular Devices).

2.11. Concanavalin A-induced hepatitis

Concanavalin A (Sigma–Aldrich) was dissolved in pyrogen-free normal saline solution at a concentration of 2.0 mg/mL and injected intravenously at a dose of 20 mg/kg body weight to induce hepatitis, as previously described [23].

2.12. Quantitative real-time reverse transcription polymerase chain reaction (qPCR)

Total RNA of mouse liver was isolated and transcribed into cDNA using the RNeasy Plus Mini Kit (Qiagen, Hilden, Germany) and Superscript III reverse transcriptase (Life Technologies) according to the manufacturer's instructions. qPCR was performed using THUNDERBIRD SYBR qPCR Mix (Toyobo, Osaka, Japan) on a LightCycler 480 (Roche Diagnostics GmbH). The normalization of relative expression was calculated by the comparative Ct ($2^{-\Delta\Delta Ct}$) method with 18s gene expression. The primer sequences used

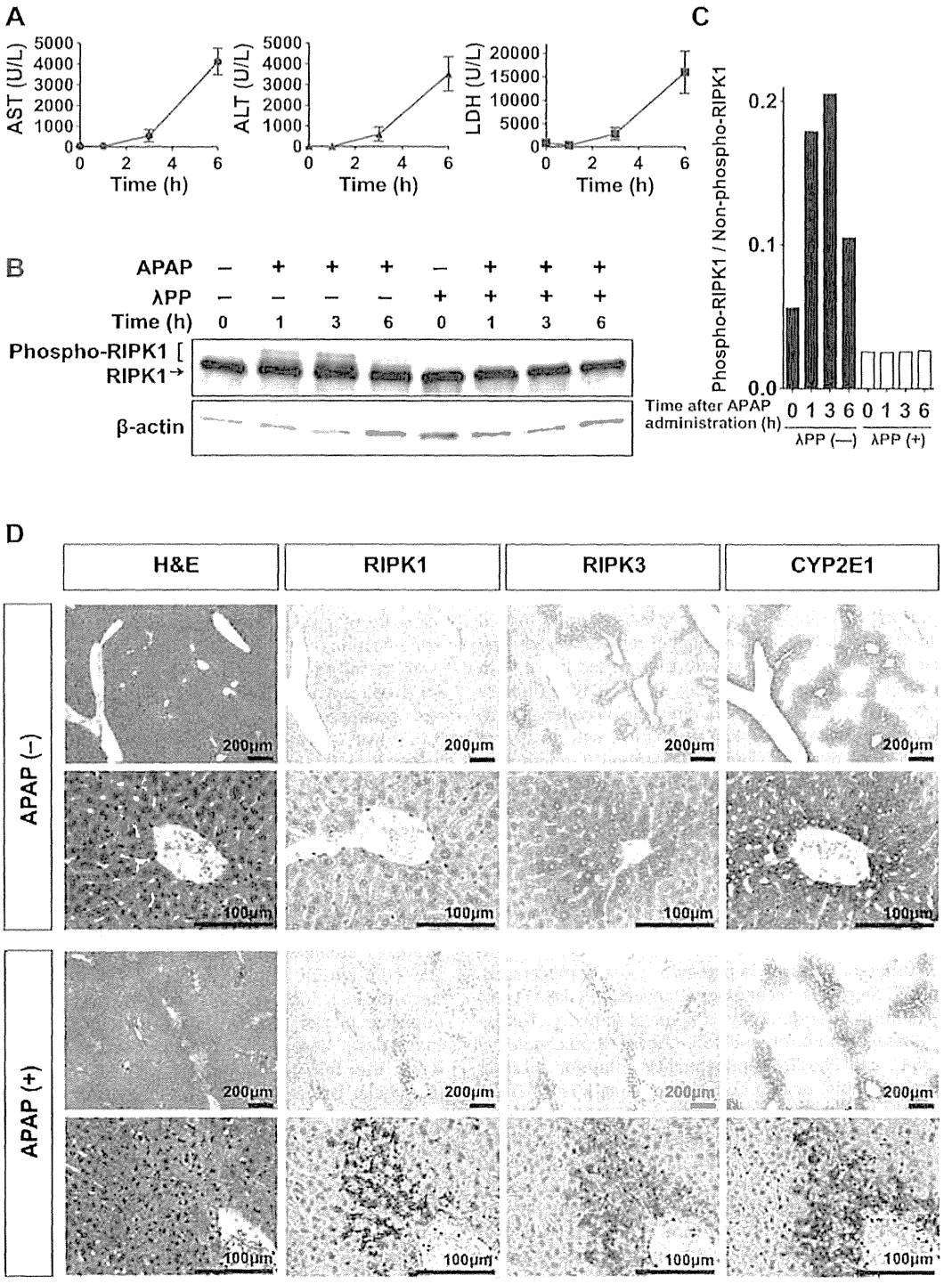

Fig. 1. RIPK1 activation during acetaminophen (APAP)-induced liver injury and localization of RIPK1 and RIPK3 in the liver. (A) Time course for the development of APAP toxicity ($n = 3$ animals per time point). (B) Protein blotting of RIPK1 and phospho-RIPK1. (C) Densitometric analysis of blotted proteins of SDS–PAGE (B). (D) Localization of RIPK1, RIPK3, and CYP2E1 in mouse liver with or without APAP administration. Liver sections stained with hematoxylin and eosin (H and E) are also shown.

were as follows: TNF, forward 5′-AGGGTCTGGGCCATAGAACT-3′, reverse 5′-CCACCACGCTCTTCTGTCTAC-3′; Heme Oxygenase-1, forward 5′-CACAGATGGCGTCACTTCGTC-3′, reverse 5′-GTGAG GACCCACTGGAGGAG-3′; 18s, forward 5′-AGTCCCTGCCCTTTGTAC-ACA-3′, reverse 5′-CGATCCGAGGGCCTCACTA-3′.

2.13. Statistical analyses

Results are presented as means ± standard errors of the mean. The two groups were compared using the unpaired Student's *t* test and analysis of variance, where appropriate. Multiple groups were

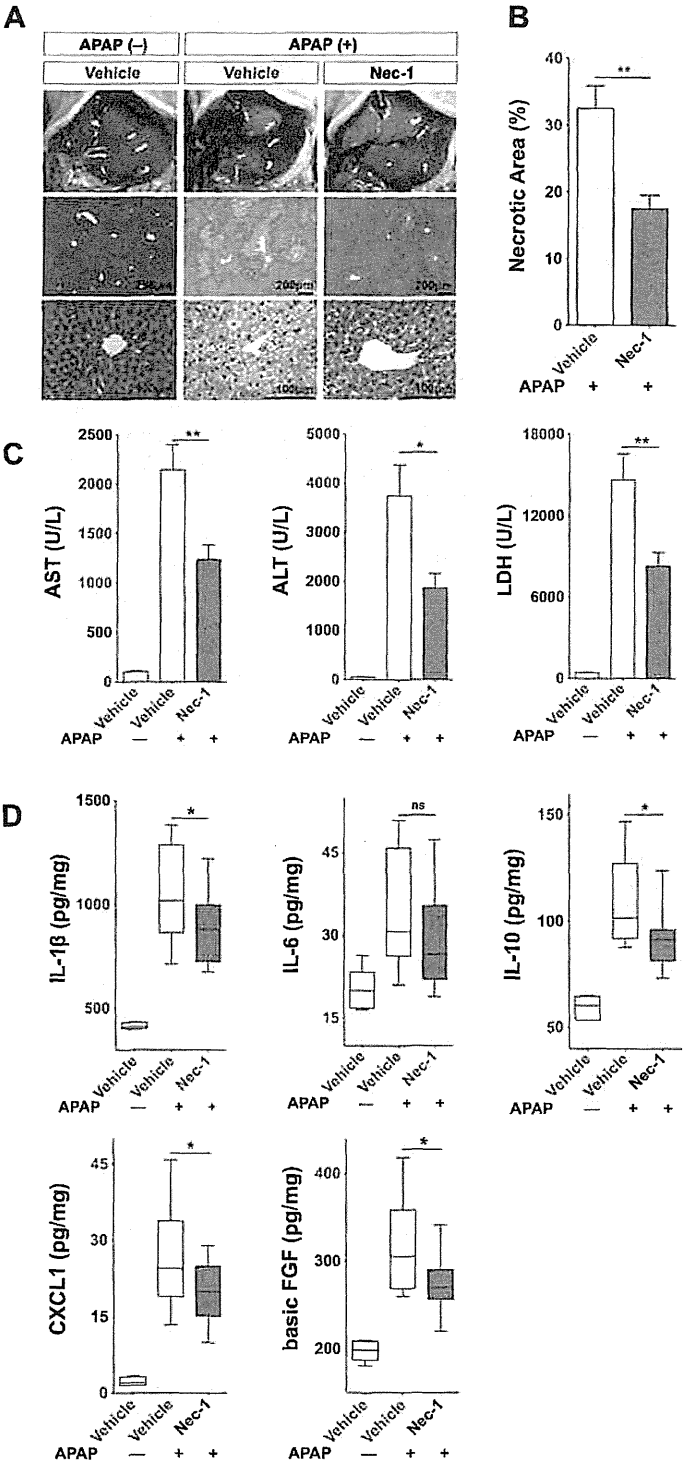

Fig. 2. Specific inhibition of RIPK1 kinase by Nec-1 protects mice against acetaminophen (APAP)-induced hepatic injury. (A) Macroscopical and histological examination of Nec-1 protection against APAP. Representative hematoxylin and eosin-stained liver sections are shown. (B) The percent necrotic area for vehicle-treated ($n = 9$) or Nec-1-treated ($n = 9$) mice was determined by random evaluation of each hematoxylin and eosin-stained sections. (C) Serum AST, ALT, and LDH levels ($n = 21$–22). (D) Hepatic IL-1β, IL-6, IL-10, CXCL1, and basic FGF expression was measured by bead-based immunoassays ($n = 12$). $^{*}P < 0.05$, $^{**}P < 0.01$.

compared by one-way analysis of variance using the Tukey's multiple comparison test or the Kruskal–Wallis test followed by Dunn's multiple comparisons. A probability (P) value <0.05 was considered statistically significant. All statistical analyses were performed using GraphPad Prism version 5.0 software (GraphPad Software, Inc., La Jolla, CA, USA).

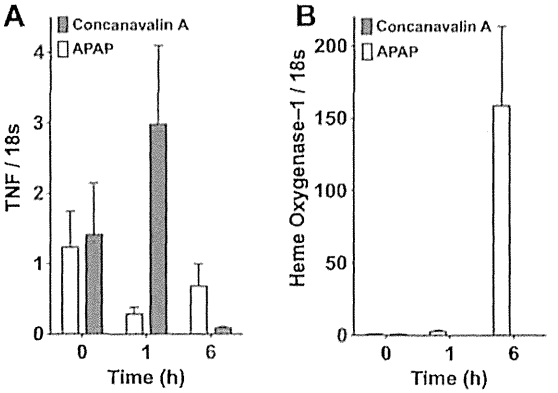

Fig. 3. Differential regulation of TNF vs. heme oxygenase-1 mRNA expression in APAP- and concanavalin A-induced acute hepatic injury; mRNA expression of TNF (A) and heme oxygenase-1 (B) in liver tissues. Mice were administered with APAP (800 mg/kg, intraperitoneal injection, $n = 3$ per time point) or concanavalin A (20 mg/kg, intravenous injection, $n = 4$ per time point) to induce hepatic injury. Liver samples were harvested before or 1 h and 6 h after administration. Total RNA was prepared at each indicated time point and subjected to quantitative RT-PCR. Error bars show standard error of the mean.

3. Results

3.1. APAP-induced hepatotoxicity is associated with RIPK1 activation

Initially, we confirmed the time-dependent development of APAP-induced liver damage in C57BL/6 mice with a single dose of APAP (800 mg/kg). Serum AST, ALT, and LDH levels were increased to 3–6 h after APAP administration (Fig. 1A). Next, we evaluated RIPK1 expression and activation in mouse liver to examine the possibility that RIPK-dependent necrosis is involved in APAP-induced hepatotoxicity. RIPK1 protein expression was observed even in the absence of APAP administration, where APAP administration led to the induction of slow-migrating bands at 1–3 h (Fig. 1B). The upper RIPK1 bands disappeared following treatment of the cell lysates with λPP (Fig. 1B and C), indicating that those bands represented phosphorylated-RIPK1, which has been characterized as a hall mark of RIPK1 activation [24]. These data imply the possibility that RIPK1 may play a role in APAP-induced hepatocyte injury in mice and that RIPK-dependent necrosis is involved in this model. To further assess the involvement of RIPK-dependent necrosis, the localization of RIPK1 and RIPK3 was immunohistochemically investigated (Fig. 1D). RIPK3 was strongly expressed in hepatocytes around the central vein area and co-localized with CYP2E1, which is a key enzyme in the conversion of APAP to highly reactive NAPQI, whereas RIPK1 was diffusely expressed in hepatocytes throughout the entire liver. Of note, APAP-induced cell death mainly proceeds around the central vein [25], where CYP2E1, RIPK1, and RIPK3 expression occur. Interestingly, Dot-like RIPK1 expression was strongly induced in and around the necrotic area after APAP administration (Fig. 1D). These results also suggested that APAP-induced cell death in mice involved RIPK-dependent necrosis.

3.2. Nec-1 protects against APAP-induced hepatic injury in vivo

To clearly demonstrate the involvement of RIPK1-dependent necrosis in APAP-induced hepatotoxicity, we utilized a murine model of APAP-induced ALF. Hepatic injury was induced by intraperitoneal injection of APAP. Mice that were administered DMSO as a vehicle showed severe hepatic injury, as assessed histologically by hematoxylin and eosin staining (Fig. 2A). We observed increased numbers of swollen hepatocytes around the central vein (Fig. 2A), and severe hemorrhage was visible in the perinecrotic area (Fig. 2A). However, mice treated with Nec-1 showed mild injury, and the necrotic area was localized only to the pericentral vein area (Fig. 2A and B). These results were confirmed by serum transaminase and LDH levels, i.e., Nec-1 showed a significant protective effect against APAP-induced hepatic injury (Fig. 2C). Without administration of APAP, no significant difference was observed between hepatocytes treated either with the vehicle alone or 50 μM Nec-1 alone (data not shown). Nec-1 significantly decreased the production of the inflammatory and regenerative cytokines IL-1β, IL-10, CXCL1, and basic FGF as compared with the vehicle (Fig. 2D). Although, no significant difference was detected in IL-6 concentrations, a tendency towards decreased expression was observed (Fig. 2D). TNF induction, which is a virulence determinant of concanavalin A- and LPS/D-galactosamine-induced hepatitis [23,26–28], was not observed in our experimental ALF settings, i.e., the liver samples were harvested within 6 h after APAP administration (Fig. 3A). However, heme oxygenase-1, which is known to be induced by APAP, was observed even in the early phase of liver injury [29] (Fig. 3B), which is in agreement with previous reports that showed APAP-induction of TNF only occurred in the later phase and not in the acute phase [30,31].

Altogether, these results clearly demonstrated that RIPK1-specific agent Nec-1 has a protective effect against APAP-induced hepatotoxicity and that APAP-induced cell death is due, at least partly, to RIPK-dependent necrosis.

3.3. Nec-1 inhibits ROS production and suppresses mitochondrial dysfunction in APAP-damaged hepatocytes

To investigate the mechanism of how RIPK1 inhibition protects hepatocytes from APAP-induced regulated necrosis, we isolated primary hepatocytes and performed cell-based *in vitro* assays. In agreement with our *in vivo* findings, RIPK1-phosphorylation also increased in APAP-treated hepatocytes in a time-dependent manner (Figs. 1B and 4A). Nec-1 protected primary hepatocytes from APAP-induced cytotoxicity in a dose-dependent manner, as shown by the reduction of LDH in the supernatant (Fig. 4B) and by increased cell viability (Fig. 4C). The protective effect of Nec-1 against APAP-induced cell death was also observed microscopically, as assessed by staining with the membrane-impermeant fluorescent molecule PI to evaluate cell death and the membrane-permeant fluorescent dye Hoechst 33342 to stain cell nuclei (Fig. 4D).

Next, we compared CYP2E1 expression levels to determine whether the Nec-1 protective effect against hepatic injury resulted from altered APAP metabolism. Therefore, we could not detect any significant differences in CYP2E1 expression levels between Nec-1- and vehicle-treated hepatocytes during APAP-induced hepatocyte death (0–6 h post APAP-treatment) (Fig. 4E and F). In addition, we examined the total GSH to assess the detoxification status of the cells, because highly reactive NAPQI is detoxified primarily by GSH conjugation. Nevertheless, total GSH levels in APAP-injured hepatocytes decreased with time regardless of Nec-1 treatment (Fig. 4G).

After GSH depletion, it is considered that NAPQI becomes hepatotoxic by binding to cellular macromolecules, which leads to cellular organ damage including mitochondrial dysfunction through ROS generation [32]. Therefore, we examined the effect of Nec-1 on intracellular ROS induction by APAP and found that Nec-1 suppressed the cellular ROS levels in APAP-treated hepatocytes to levels similar to those in APAP-untreated hepatocytes (Fig. 4H). Similarly, Nec-1 suppressed the mitochondrial ROS induction in APAP-treated hepatocytes, as determined using MitoSOX Red, whereas mitochondrial ROS were strongly induced in APAP-damaged hepatocytes treated with the vehicle alone (Fig. 4I).

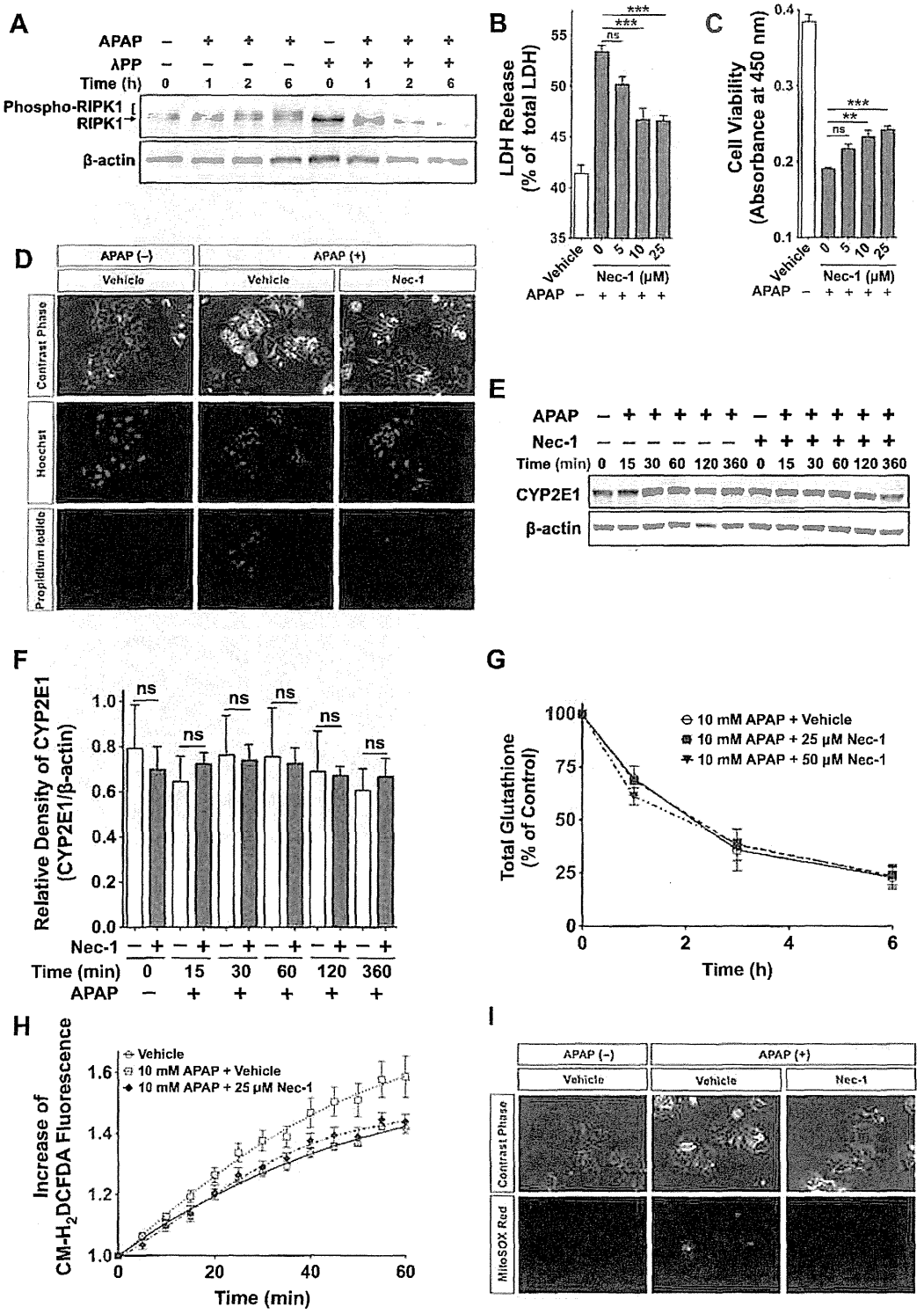

Fig. 4. Nec-1 inhibits ROS production and suppresses mitochondrial dysfunction in acetaminophen (APAP)-damaged hepatocytes without affecting CYP2E1 and cellular GSH levels. (A) APAP-induced activation of RIPK1. SDS–PAGE of RIPK1 and phospho-RIPK1 in cultured mouse hepatocytes with or without λPP is shown. (B) Effect of Nec-1 on APAP-induced LDH release (18 h after APAP treatment, $n = 6$). (C) Effect of Nec-1 on APAP-induced hepatocyte death (18 h after APAP treatment, $n = 6$) (D) Microscopical analysis of hepatocytes with or without Nec-1 (6 h after APAP treatment). (E) SDS–PAGE of CYP2E1 expression (F) Densitometric analysis of (E) ($n = 3$). (G) APAP-induced depletion of cellular GSH levels in primary hepatocytes with 25 μM and 50 μM Nec-1 or the vehicle. Data are expressed as percent of non-APAP-treated controls ($n = 3$). (H) The redox-sensitive dye CM-H_2DCFDA (10 μM) was loaded for 30 min. Fluorescent signals were quantified continuously for 60 min ($n = 8$). (I) Cells were loaded with MitoSOX (2.5 μM) for 6 h and live images were captured. Pictures are representative of three different experiments. $^*P < 0.05$, $^{**}P < 0.01$, $^{***}P < 0.001$.

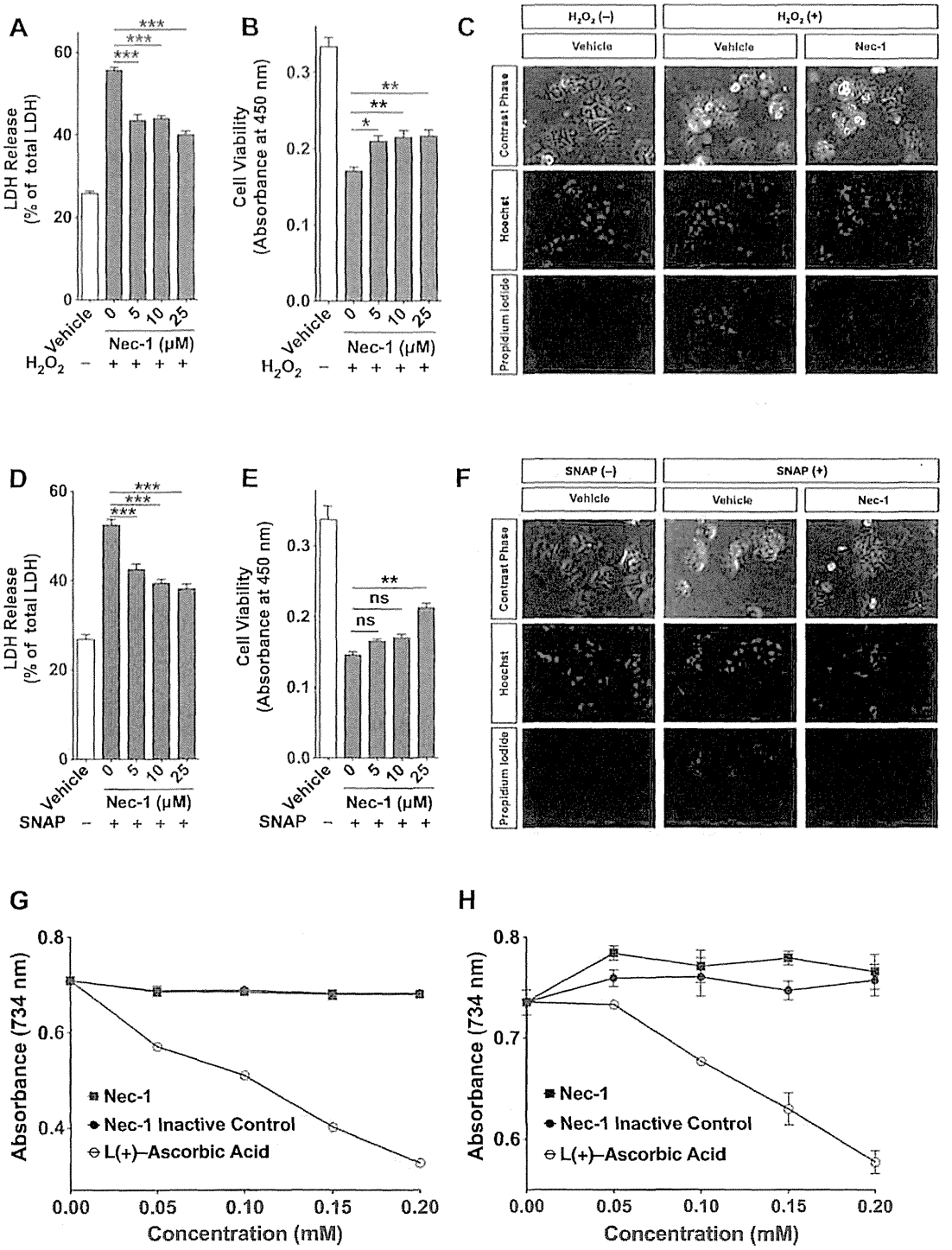

Fig. 5. RIPK1 inhibition by Nec-1 confers hepatocytes resistance to oxidative stress, isolated hepatocytes were cultured with different Nec-1 concentrations or the vehicle alone for 1 h and then treated with 250 μM H_2O_2 or 2 mM SNAP. (A and D) LDH was measured 6 h after H_2O_2 (A) or SNAP (D) administration ($n = 6$). (B and E) Cell viability was measured 6 h after H_2O_2 (B) or SNAP (E) administration using WST-8 ($n = 6$). (C and F) The cells were stained with Hoechst 33342 and propidium iodide 6 h after adding H_2O_2 (C) or SNAP (F), and then examined by fluorescent microscopy. (G and H) The antioxidant effect of Nec-1 was evaluated using the ABTS free-radical decolorization assay. An Nec-1 inactive control and L(+)-ascorbic acid were used as controls. Samples were dissolved in either distilled water (G) or ethanol (H) ($n = 6$). $^{*}P < 0.05$, $^{**}P < 0.01$, $^{***}P < 0.001$.

These findings raise the possibility that Nec-1 protects against APAP-induced hepatocyte injury by suppressing the intracellular burden of ROS formation, including mitochondrial superoxide production, without affecting CYP2E1 expression or depleting GSH.

3.4. RIPK1 inhibition confers hepatocytes resistance to oxidative stress

Extensive mitochondrial GSH depletion is associated with a significant increase in H_2O_2 released from stressed mitochondria [33].

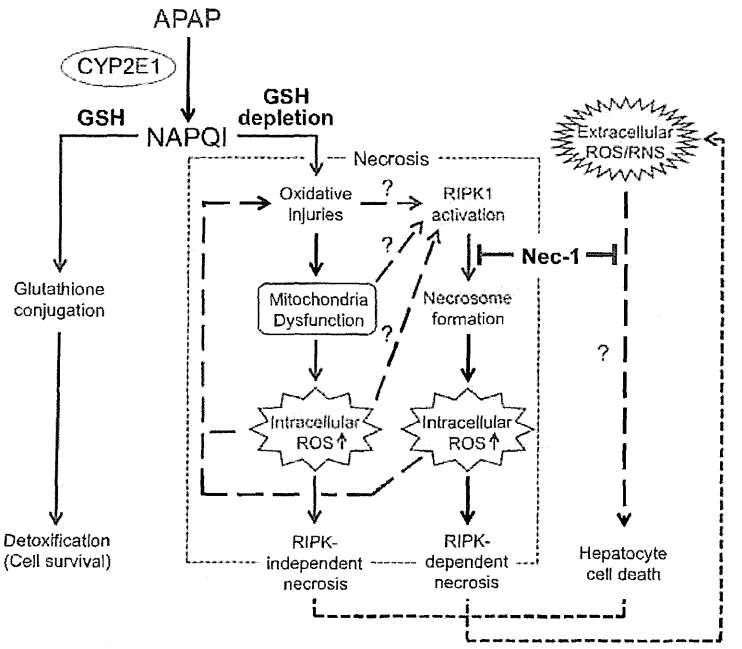

Fig. 6. Schematic illustration of the model for the protective effect(s) of Nec-1 against acetaminophen (APAP)-induced hepatocyte necrosis. APAP is converted to the highly reactive metabolite NAPQI by CYP2E1 and other cytochrome P450 enzymes (CYPs) in the liver. NAPQI is inactivated by conjugation to GSH and detoxified. However, excess NAPQI leads to GSH depletion and unconjugated NAPQI binds to cellular proteins, causing further formation of ROS. Resultant oxidative injuries, including mitochondria dysfunction, result in massive hepatic necrosis. Although the mechanism of RIPK1 activation remains unclear, Nec-1 inhibits necrosome formation and intracellular ROS production, which eventually prevent RIPK-dependent necrosis. ROS and reactive nitrogen species (RNS) produced by living cells and/or leaked from dead cells (extracellular ROS/RNS) also provoke hepatocyte cell death. By unknown mechanisms, Nec-1 also inhibits this cell death pathway.

Peroxynitrite ($ONOO^-$), which is formed by the reaction of nitric oxide (NO) with superoxide, is detoxified by GSH during APAP-induced hepatotoxicity [34]. These oxidizing agents produced in living cells and/or leaked from dead cells not only damage organs intracellularly, but may also affect neighboring cells extracellularly [35,36]. Therefore, we attempted to test whether RIPK1 inhibition influenced hepatocyte response to exogenous oxidative stress. We treated mouse hepatocytes with H_2O_2 or SNAP, which serves as a NO donor. Low SNAP concentrations provide protection from cell death in various cell types, including hepatocytes [37–39]; however, at higher concentrations, SNAP is highly toxic [39–42]. Thus, we used SNAP in a concentration range that was toxic to hepatocytes (data not shown) and found a dose-dependent protective effect of Nec-1 against exogenous oxidative stress in cell viability and LDH-release assays (Fig. 5A, B, D and E). A microscopic analysis confirmed that RIPK1 inhibition by Nec-1 protected the primary hepatocytes from exogenous oxidizing agents (Fig. 5C and F). However, there was no antioxidant activity in Nec-1 compared with L(+)-Ascorbic Acid, which is an antioxidant well-known as Vitamin C, as determined by an ABTS free-radical decolorization assay (Fig. 5G and H). This suggests that Nec-1 does not act as a scavenger for H_2O_2 or SNAP. These results collectively indicate that RIPK1 inhibition not only suppresses ROS production in hepatocytes but also ameliorates hepatocyte damage caused by extracellular ROS (Fig. 6); although the exact mechanism remains to be addressed.

4. Discussion

Our results demonstrate that RIPK-dependent necrosis is involved in the pathological manifestation of APAP-induced acute liver damage. Indeed, RIPK1 inhibition by Nec-1 showed a protective effect against APAP-induced hepatocyte injury both *in vivo* and *in vitro*. The *in vitro* studies revealed that RIPK1 inhibition reduces APAP-induced ROS production, which is one of the main causes of APAP-induced hepatocyte damage (Fig. 5) [43], whereas CYP2E1 expression and APAP-induced GSH exhaustion were unaffected (Fig. 4E–G). A pathological examination of the liver before and after APAP injury demonstrated co-localization of RIPK1 with RIPK3 and CYP2E1 in hepatocytes around the central vein area (Fig. 1D), which is the most vulnerable area for APAP-induced hepatocyte injury [25], also supporting the notion that RIPK-dependent mechanisms operate in APAP liver injury. Furthermore, although Nec-1 has no antioxidant activity (Fig. 4G and H) [14], we found that Nec-1-treated hepatocytes acquired resistance to oxidative stress. This resistance mechanism remains to be elucidated; however, the resistance would be beneficial to further protect against APAP-induced liver damage, because extracellular ROS increase in response to initial hepatocyte cell death [35,36], and those ROS together with inflammatory cytokines lead to secondary hepatocyte damage [44] (Figs. 5 and 6).

APAP-induced cell death is predominantly necrotic [6]. Our results clearly demonstrated that APAP-induced necrosis includes, if not all, regulated forms of necrosis that are a druggable target of RIPK1 inhibitors (Fig. 6). Nec-1 has a short half-life span [45], but demonstrated efficacy against APAP-induced ALF. Thus, the development of inhibitors with better pharmacokinetic properties may pave the way for therapeutic intervention of human APAP-induced ALF, for which efficient treatment is truly required.

Author contributions

K. Takemoto, K.I., E.H. and M.A. designed the study. K. Takemoto, K.I., M.T., and N.N. performed experiments and analyzed data. S.O., K. Toriguchi, K. Tanabe, H.T., S. Seo, K. Taura, K.M., S. Saji and S.U. provided technical and analytical assistance. K. Takemoto, E.H., N.T. and M.A. wrote and edited the manuscript.

Conflicts of interest

M.A. receives a grant from Innovation Center for Immunoregulation and Therapeutics (AK Project). However, the study was designed, conducted, analyzed, and reported independently of the funding. No other potential conflict of interest relevant to this article was reported.

Acknowledgments

We are grateful to Dr. Yuji Takemoto and Dr. Takeshi Watanabe for their continuous support and fruitful discussion. This work was supported in part by a grant from the Japanese Ministry of Health, Labour and Welfare (K.I., N.T., S.U., and M.A.); a Grant-in-Aid for Young Scientists (M.A.) and a Grant-in-Aid for Challenging Exploratory Research (M.A.) from Japan Society for the Promotion of Science; and a grant from the Kanae Foundation for the Promotion of Medical Science (M.A.).

References

[1] Kaufman, D.W., Kelly, J.P., Rosenberg, L., Anderson, T.E. and Mitchell, A.A. (2002) Recent patterns of medication use in the ambulatory adult population of the United States: the Slone survey. JAMA 287, 337–344.
[2] Larson, A.M., Polson, J., Fontana, R.J., Davern, T.J., Lalani, E., Hynan, L.S., Reisch, J.S., Schiodt, F.V., Ostapowicz, G., Shakil, A.O., Lee, W.M. and Grp, A.L.F.S. (2005) Acetaminophen-induced acute liver failure: results of a United States multicenter, prospective study. Hepatology 42, 1364–1372.
[3] Bernal, W., Auzinger, G., Dhawan, A. and Wendon, J. (2010) Acute liver failure. Lancet 376, 190–201.
[4] Dahlin, D.C., Miwa, G.T., Lu, A.Y. and Nelson, S.D. (1984) N-Acetyl-p-benzoquinone imine: a cytochrome P-450-mediated oxidation product of acetaminophen. Proc. Natl. Acad. Sci. U.S.A. 81, 1327–1331.
[5] Kon, K., Kim, J.S., Jaeschke, H. and Lemasters, J.J. (2004) Mitochondrial permeability transition in acetaminophen-induced necrosis and apoptosis of cultured mouse hepatocytes. Hepatology 40, 1170–1179.
[6] Gujral, J.S., Knight, T.R., Farhood, A., Bajt, M.L. and Jaeschke, H. (2002) Mode of cell death after acetaminophen overdose in mice: apoptosis or oncotic necrosis? Toxicol. Sci. 67, 322–328.
[7] El-Hassan, H., Anwar, K., Macanas-Pirard, P., Crabtree, M., Chow, S.C., Johnson, V.L., Lee, P.C., Hinton, R.H., Price, S.C. and Kass, G.E. (2003) Involvement of mitochondria in acetaminophen-induced apoptosis and hepatic injury: roles of cytochrome c, Bax, Bid, and caspases. Toxicol. Appl. Pharmacol. 191, 118–129.
[8] Galluzzi, L., Vitale, I., Abrams, J.M., Alnemri, E.S., Baehrecke, E.H., Blagosklonny, M.V., Dawson, T.M., Dawson, V.L., El-Deiry, W.S., Fulda, S., Gottlieb, E., Green, D.R., Hengartner, M.O., Kepp, O., Knight, R.A., Kumar, S., Lipton, S.A., Lu, X., Madeo, F., Malorni, W., Mehlen, P., Nuñez, G., Peter, M.E., Piacentini, M., Rubinsztein, D.C., Shi, Y., Simon, H.U., Vandenabeele, P., White, E., Yuan, J., Zhivotovsky, B., Melino, G. and Kroemer, G. (2012) Molecular definitions of cell death subroutines: recommendations of the Nomenclature Committee on Cell Death 2012. Cell Death Differ. 19, 107–120.
[9] Cho, Y.S., Challa, S., Moquin, D., Genga, R., Ray, T.D., Guildford, M. and Chan, F.K. (2009) Phosphorylation-driven assembly of the RIP1–RIP3 complex regulates programmed necrosis and virus-induced inflammation. Cell 137, 1112–1123.
[10] Vandenabeele, P., Declercq, W., Van Herreweghe, F. and Vanden Berghe, T. (2010) The role of the kinases RIP1 and RIP3 in TNF-induced necrosis. Sci. Signal. 3.
[11] Wang, Z., Jiang, H., Chen, S., Du, F. and Wang, X. (2012) The mitochondrial phosphatase PGAM5 functions at the convergence point of multiple necrotic death pathways. Cell 148, 228–243.
[12] Degterev, A., Hitomi, J., Germscheid, M., Ch'en, I.L., Korkina, O., Teng, X., Abbott, D., Cuny, G.D., Yuan, C., Wagner, G., Hedrick, S.M., Gerber, S.A., Lugovskoy, A. and Yuan, J. (2008) Identification of RIP1 kinase as a specific cellular target of necrostatins. Nat. Chem. Biol. 4, 313–321.
[13] Vandenabeele, P., Galluzzi, L., Vanden Berghe, T. and Kroemer, G. (2010) Molecular mechanisms of necroptosis: an ordered cellular explosion. Nat. Rev. Mol. Cell Biol. 11, 700–714.
[14] Degterev, A., Huang, Z., Boyce, M., Li, Y., Jagtap, P., Mizushima, N., Cuny, G.D., Mitchison, T.J., Moskowitz, M.A. and Yuan, J. (2005) Chemical inhibitor of nonapoptotic cell death with therapeutic potential for ischemic brain injury. Nat. Chem. Biol. 1, 112–119.
[15] Oerlemans, M.I., Liu, J., Arslan, F., den Ouden, K., van Middelaar, B.J., Doevendans, P.A. and Sluijter, J.P. (2012) Inhibition of RIP1-dependent necrosis prevents adverse cardiac remodeling after myocardial ischemia-reperfusion in vivo. Basic Res. Cardiol. 107, 270.
[16] Nehs, M.A., Lin, C.I., Kozono, D.E., Whang, E.E., Cho, N.L., Zhu, K., Moalem, J., Moore, F.D. and Ruan, D.T. (2011) Necroptosis is a novel mechanism of radiation-induced cell death in anaplastic thyroid and adrenocortical cancers. Surgery 150, 1032–1039.
[17] Park, Y., Smith, R.D., Combs, A.B. and Kehrer, J.P. (1988) Prevention of acetaminophen-induced hepatotoxicity by dimethyl sulfoxide. Toxicology 52, 165–175.
[18] Tamaki, N., Hatano, E., Taura, K., Tada, M., Kodama, Y., Nitta, T., Iwaisako, K., Seo, S., Nakajima, A., Ikai, I. and Uemoto, S. (2008) CHOP deficiency attenuates cholestasis-induced liver fibrosis by reduction of hepatocyte injury. Am. J. Physiol. Gastrointest. Liver Physiol. 294, G498–G505.
[19] Wu, D.F., Clepan, L., Potter, B. and Cederbaum, A.I. (1990) Rapid decrease of cytochrome P-450IIE1 in primary hepatocyte culture and its maintenance by added 4-methylpyrazole. Hepatology 12, 1379–1389.
[20] Park, Y.H., Iwaisako, K., Seki, E., Inokuchi, S., Schnabl, B., Osterreicher, C.H., Kisseleva, T. and Brenner, D.A. (2011) The nicotinamide adenine dinucleotide phosphate oxidase (NOX) homologues NOX1 and NOX2/gp91(phox) mediate hepatic fibrosis in mice. Hepatology 53, 1730–1741.
[21] Kosako, H., Yamaguchi, N., Aranami, C., Ushiyama, M., Kose, S., Imamoto, N., Taniguchi, H., Nishida, E. and Hattori, S. (2009) Phosphoproteomics reveals new ERK MAP kinase targets and links ERK to nucleoporin-mediated nuclear transport. Nat. Struct. Mol. Biol. 16, 1026–1035.
[22] Re, R., Pellegrini, N., Proteggente, A., Pannala, A., Yang, M. and Rice-Evans, C. (1999) Antioxidant activity applying an improved ABTS radical cation decolorization assay. Free Radic Biol Med 26, 1231–1237.
[23] Gantner, F., Leist, M., Lohse, A.W., Germann, P.G. and Tiegs, G. (1995) Concanavalin A-induced T-cell-mediated hepatic injury in mice – the role of tumor necrosis factor. Hepatology 21, 190–198.
[24] Declercq, W., Vanden Berghe, T. and Vandenabeele, P. (2009) RP kinases at the crossroads of cell death and survival. Cell 138, 229–232.
[25] Roberts, D.W., Bucci, T.J., Benson, R.W., Warbritton, A.R., McRae, T.A., Pumford, N.R. and Hinson, J.A. (1991) Immunohistochemical localization and quantification of the 3-(cystein-S-yl)-acetaminophen protein adduct in acetaminophen hepatotoxicity. Am. J. Pathol. 138, 359–371.
[26] Maeda, S., Chang, L.F., Li, Z.W., Luo, J.L., Leffert, H. and Karin, M. (2003) IKK beta is required for prevention of apoptosis mediated by cell-bound but not by circulating TNF alpha. Immunity 19, 725–737.
[27] Pasparakis, M., Alexopoulou, L., Episkopou, V. and Kollias, G. (1996) Immune and inflammatory responses in TNF alpha-deficient mice: a critical requirement for TNF alpha in the formation of primary B cell follicles, follicular dendritic cell networks and germinal centers, and in the maturation of the humoral immune response. J. Exp. Med. 184, 1397–1411.
[28] Lehmann, V., Freudenberg, M.A. and Galanos, C. (1987) Lethal toxicity of lipopolysaccharide and tumor-necrosis-factor in normal and D-galactosamine-treated mice. J. Exp. Med. 165, 657–663.
[29] Mobasher, M.A., Gonzalez-Rodriguez, A., Santamaria, B., Ramos, S., Martin, M.A., Goya, L., Rada, P., Letzig, L., James, L.P., Cuadrado, A., Martin-Perez, J., Simpson, K.J., Muntane, J. and Valverde, A.M. (2013) Protein tyrosine phosphatase 1B modulates GSK3 beta/Nrf2 and IGFIR signaling pathways in acetaminophen-induced hepatotoxicity. Cell Death Dis 4.
[30] Gardner, C.R., Laskin, J.D., Dambach, D.M., Sacco, M., Durham, S.K., Bruno, M.K., Cohen, S.D., Gordon, M.K., Gerecke, D.R., Zhou, P. and Laskin, D.L. (2002) Reduced hepatotoxicity of acetaminophen in mice lacking inducible nitric oxide synthase: potential role of tumor necrosis factor-alpha and interleukin-10. Toxicol. Appl. Pharmacol. 184, 27–36.
[31] Blazka, M.E., Wilmer, J.L., Holladay, S.D., Wilson, R.E. and Luster, M.I. (1995) Role of proinflammatory cytokines in acetaminophen hepatotoxicity. Toxicol. Appl. Pharmacol. 133, 43–52.
[32] Jaeschke, H. (1990) Glutathione disulfide formation and oxidant stress during acetaminophen-induced hepatotoxicity in mice in vivo: the protective effect of allopurinol. J. Pharmacol. Exp. Ther. 255, 935–941.
[33] Han, D., Canali, R., Rettori, D. and Kaplowitz, N. (2003) Effect of glutathione depletion on sites and topology of superoxide and hydrogen peroxide production in mitochondria. Mol. Pharmacol. 64, 1136–1144.
[34] Sies, H., Sharov, V.S., Klotz, L.O. and Briviba, K. (1997) Glutathione peroxidase protects against peroxynitrite-mediated oxidations. A new function for selenoproteins as peroxynitrite reductase. J. Biol. Chem. 272, 27812–27817.
[35] Laskin, J.D., Heck, D.E., Gardner, C.R. and Laskin, D.L. (2001) Prooxidant and antioxidant functions of nitric oxide in liver toxicity. Antioxid. Redox Signal. 3, 261–271.
[36] Dragomir, A.C., Laskin, J.D. and Laskin, D.L. (2011) Macrophage activation by factors released from acetaminophen-injured hepatocytes: potential role of HMGB1. Toxicol. Appl. Pharmacol. 253, 170–177.
[37] Farinelli, S.E., Park, D.S. and Greene, L.A. (1996) Nitric oxide delays the death of trophic factor-deprived PC12 cells and sympathetic neurons by a cGMP-mediated mechanism. J. Neurosci. 16, 2325–2334.
[38] Hatano, E., Bennett, B.L., Manning, A.M., Qian, T., Lemasters, J.J. and Brenner, D.A. (2001) NF-kappaB stimulates inducible nitric oxide synthase to protect mouse hepatocytes from TNF-alpha- and Fas-mediated apoptosis. Gastroenterology 120, 1251–1262.
[39] Shen, Y.H., Wang, X.L. and Wilcken, D.E.L. (1998) Nitric oxide induces and inhibits apoptosis through different pathways. FEBS Lett. 433, 125–131.
[40] Bal-Price, A. and Brown, G.C. (2000) Nitric-oxide-induced necrosis and apoptosis in PC12 cells mediated by mitochondria. J. Neurochem. 75, 1455–1464.
[41] Figueroa, S., Oset-Gasque, M.J., Arce, C., Martinez-Honduvilla, C.J. and Gonzalez, M.P. (2006) Mitochondrial involvement in nitric oxide-induced cellular death in cortical neurons in culture. J. Neurosci. Res. 83, 441–449.

[42] Uchiyama, T., Otani, H., Okada, T., Ninomiya, H., Kido, M., Imamura, H., Nogi, S. and Kobayashi, Y. (2002) Nitric oxide induces caspase-dependent apoptosis and necrosis in neonatal rat cardiomyocytes. J. Mol. Cell. Cardiol. 34, 1049–1061.
[43] Jaeschke, H., McGill, M.R. and Ramachandran, A. (2012) Oxidant stress, mitochondria, and cell death mechanisms in drug-induced liver injury: lessons learned from acetaminophen hepatotoxicity. Drug Metab. Rev. 44, 88–106.
[44] Mosser, D.M. and Edwards, J.P. (2008) Exploring the full spectrum of macrophage activation. Nat. Rev. Immunol. 8, 958–969.
[45] Degterev, A., Maki, J.L. and Yuan, J. (2013) Activity and specificity of necrostatin-1, small-molecule inhibitor of RIP1 kinase. Cell Death Differ. 20, 366.

Curr Pathobiol Rep (2014) 2:209–215
DOI 10.1007/s40139-014-0057-8

MYOFIBROBLAST (TATIANA KISSELEVA, SECTION EDITOR)

Strategies to Detect Hepatic Myofibroblasts in Liver Cirrhosis of Different Etiologies

Keiko Iwaisako · Kojiro Taura · Yukinori Koyama · Kenji Takemoto · Masataka Asagiri

Published online: 14 September 2014

Abstract Liver cirrhosis, a late stage of hepatic fibrosis, is an increasing cause of morbidity and mortality worldwide. Hepatic fibrosis is mainly caused by alcoholic or non-alcoholic steatohepatitis, chronic viral hepatitis, or autoimmune and biliary diseases. Myofibroblasts, which are absent from the normal liver, are differentiated from heterogeneous cell populations in response to a liver injury of any etiology and produce the extracellular matrix. Hepatic stellate cells are considered the main source of myofibroblasts. However, the origin of hepatic myofibroblasts remains unresolved, and despite considerable research, only a limited success has been achieved by existing anti-fibrotic therapies. The question remains whether these limitations are caused by lack of attention to the critical targets, the myofibroblasts derived from cells of other mesenchymal origins. Therefore, identifying the origin of myofibroblasts may provide insight into the mechanisms underlying liver fibrosis, and may lead to the development of more effective therapies. This review will examine our current strategies for detecting hepatic myofibroblasts of different origins.

K. Iwaisako (✉)
Department of Target Therapy Oncology, Kyoto University Graduate School of Medicine, 54 Kawaharacho, Shogoin, Sakyo-Ku, Kyoto 606-8507, Japan
e-mail: iwaisako@kuhp.kyoto-u.ac.jp

K. Taura · Y. Koyama · K. Takemoto
Division of Hepato-Biliary-Pancreatic and Transplant Surgery, Department of Surgery, Kyoto University Graduate School of Medicine, Kyoto 606-8507, Japan

K. Takemoto · M. Asagiri
Innovation Center for Immunoregulation and Therapeutics, Graduate School of Medicine, Kyoto University, Kyoto 606-8507, Japan

Keywords Liver cirrhosis · Hepatic fibrosis · Myofibroblasts · Hepatic stellate cells · Portal fibroblasts

Introduction

Liver cirrhosis (LC) is a major, life-threatening health problem worldwide. LC results from liver injuries of numerous different etiologies, causing hepatocyte damage, hepatic inflammation, and fibrogenesis [1]. LC can lead to the development of hepatocellular carcinoma [2]. LC is histologically characterized by increased deposition in and altered composition of the extracellular matrix (ECM) and the appearance of regenerative nodules. The destruction of the normal architecture of the liver and the loss of its functional hepatocytes prevent the liver from performing its normal detoxification, synthesis, and metabolic functions, eventually leading to portal hypertension and liver failure. From a clinical standpoint, LC is regarded as an end stage disease that leads to death, unless a liver transplant is performed [3]. However, several problems are associated with liver transplantation, such as a shortage of donors, post-transplant rejection, operative risk, and high costs.

Recently, it has become increasingly clear that hepatic fibrosis is reversible if its causative agents are successfully targeted; this has proved to be the most effective treatment for LC thus far [4]. However, the underlying causative agents are treatable only in subsets of patients with liver disease. Although there has been considerable research on liver fibrosis, there are no specific treatments for this condition. An ideal anti-fibrosis therapy would be specific for fibrogenic cells in the liver and be effective in attenuating excessive ECM deposition.

Myofibroblasts are the main effector cells in the fibrotic liver. In both experimental and clinical liver fibrosis cases, myofibroblasts appear and produce ECM at the site of the hepatic injury. The activation of ordinarily quiescent hepatic stellate cells (HSCs) into myofibroblasts is considered a major pathway of hepatic fibrogenesis associated with liver injury and has thus dominated the focus of studies on liver fibrosis [5]. The activated HSCs or their resulting myofibroblasts were the first major cell type in the liver to be identified as prominent in producing ECM in the injured liver [6]. Currently, at least three sources of myofibroblasts in liver fibrosis have been proposed. The hepatic resident mesenchymal cells [7], consisting of the quiescent HSCs and the portal fibroblasts, can differentiate into myofibroblasts. Then, bone-marrow derived cells, consisting of fibrocytes and mesenchymal stem cells in the peripheral blood, can be recruited to the injured liver to differentiate into myofibroblasts. Recent studies have demonstrated that bone-marrow derived cells make only a small contribution to the myofibroblast population in experimental liver fibrosis. Instead, fibrocytes may play a crucial role in the initiation of immune response during the earliest phases of tissue injury [8•]. Finally, hepatic progenitor cells, hepatocytes, cholangiocytes, and hepatic sinusoidal endothelial cells have been proposed to differentiate into myofibroblasts through epithelial or endothelial mesenchymal transition (EMT). Although primary hepatocytes can undergo EMT in vitro, it is extremely hard to detect hepatic myofibroblasts originating from epithelial or endothelial cells through EMT in vivo [9]. Thus, the main sources of hepatic myofibroblasts in liver fibrosis are the hepatic resident mesenchymal cells, consisting of the HSCs and portal fibroblasts. The most widely used and accessible marker of myofibroblasts are the de novo expression of α-smooth muscle actin (α-SMA). However, no reliable markers have yet been identified for distinguishing HSCs from portal fibroblasts after myofibroblastic differentiation. The contribution of portal fibroblasts to hepatic fibrosis is not well understood mainly because of the difficulties in distinguishing and isolating them.

Development of liver fibrosis and cirrhosis is associated with deposition of ECM, in which Collagen Type I is the most abundant [10]. Transgenic Colagen-α1(I)-GFP mice have been generated a decade ago. In these mice expression of GFP is driven by Collagen-α1(I) promoter, and therefore, expression of GFP is observed in cells that upregulate Collagen Type I. Our current review will summarize the recent results obtained from transgenic reporter mice and novel flow cytometry protocols developed to distinguish HSC- and portal fibroblast-derived myofibroblasts and quantify their relative contributions to hepatic fibrosis.

Fibrotic Cascade in the Liver

Once hepatic epithelial cells (hepatocytes and/or cholangiocytes) are damaged by any cause, inflammatory mediators are released to initiate a series of responses to liver injury. Inflammatory cells recruited to the site of injury phagocytose necrotic or apoptotic cells and amplify the inflammatory response by releasing pro-inflammatory cytokines, such as tumor necrosis factor-α (TNF-α), interleukin-6 (IL-6), and interleukin-1 beta (IL-1β), and by recruiting T cells [11]. The hepatic mesenchymal precursor cells of myofibroblasts are activated and differentiated by growth factors and cytokines including transforming growth factor-beta (TGF-β), platelet-derived growth factor (PDGF), and interleukin-13 (IL-13). TGF-β drives myofibroblast activation and ECM synthesis. PDGF stimulates HSC proliferation through its positive feedback mechanism involved in the autocrine and paracrine effect. IL-13 has been also implicated in stimulation of TGF-β synthesis in cells [12].

Immune cells play a pivotal role in the development of hepatic fibrosis. In experimentally induced fibrosis, the balance between Th1 and Th2 cells is important for the fibrotic response. For example, C57BL/6 mice (in which a Th1 cell response predominates) have a lower fibrotic reaction than BALB/c mice (in which a Th2 cell response predominates) [13]. Recently, increasing evidence has suggested an emerging novel role of T cell subsets, including Th17, Treg, and δγT cells, in the fibrotic process [14]. However, further studies are needed to fully elucidate their functions.

Hepatic fibrosis is a dynamic process and can be considered a part of the healing response to liver injury. The ECM is not stable, but is constantly synthesized and degraded by proteolytic enzymes such as the matrix metalloproteinases (MMP) or collagenases. The reversibility of mild to moderate hepatic fibrosis is now a reality in patients whose etiology has been successfully treated. In clinical practice, studies of antiviral treatments for hepatitis C have showed that fibrosis is reversible after a sustained virologic response [15]. However, there is no unequivocal evidence for a complete reversal of severe cirrhosis with regenerative nodules and dense fibrotic septa. Current clinical studies based on liver biopsies have showed that the matrix enzyme lysyl oxidase–like-2 (LOXL2) increased in the fibrotic liver and was limited in the healthy liver. LOXL2 catalyzes the first step in the formation of crosslinks in fibrillar collagen. The extensiveness of the crosslinks observed in severe fibrosis and cirrhosis prevent their degradation by collagenases [16].